

# CHALMERS



## Implementation of adhesion and non-linear contact stiffness in a numerical model for dynamic tyre/road contact

*Master of Science Thesis in the Master's Programme Sound and Vibration*

JULIA WINROTH

Department of Civil and Environmental Engineering  
*Division of Applied Acoustics*  
*Vibroacoustic group*  
CHALMERS UNIVERSITY OF TECHNOLOGY  
Göteborg, Sweden 2010  
Master's Thesis 2010:8



MASTER'S THESIS 2010:8

# Implementation of adhesion and non-linear contact stiffness in a numerical model for dynamic tyre/road contact

*Master of Science Thesis in the Master's Programme Sound and Vibration*

JULIA WINROTH

Department of Civil and Environmental Engineering  
*Division of Applied Acoustics*  
*Vibroacoustic group*  
CHALMERS UNIVERSITY OF TECHNOLOGY  
Göteborg, Sweden 2010

Implementation of adhesion and non-linear contact stiffness in a numerical model for dynamic tyre/road contact

© JULIA WINROTH, 2010

Examensarbete / Institutionen för bygg- och miljöteknik,  
Chalmers tekniska högskola 2010:8

Department of Civil and Environmental Engineering  
Division of Applied Acoustics  
Vibroacoustic group  
Chalmers University of Technology  
SE-412 96 Göteborg  
Sweden  
Telephone: + 46 (0)31-772 1000

Printed by Chalmers Reproservice  
Göteborg, Sweden, 2010

Implementation of adhesion and non-linear contact stiffness in a numerical model for dynamic tyre/road contact  
Master of Science Thesis in the Master's Programme Sound and Vibration

JULIA WINROTH

Department of Civil and Environmental Engineering

Division of Applied Acoustics

Vibroacoustic group

Chalmers University of Technology

### **Abstract**

Numerical tyre/road contact models including the effects of adhesion are of interest both for fundamental understanding of the interaction and for optimisation of tyre/road combinations. A previously developed numerical time-domain contact model that includes the effect of small-scale roughness is here extended to investigate adhesive forces and inertial effects of the tread. Adhesion is modelled by allowing negative forces in the force-compression relations of each pair of matching contact elements. A limiting force for which the individual contacts break is tested as a preliminary separation criterion. Numerical instabilities were found in the dynamic calculations but measures were successfully implemented to increase stability. Calculation results show that tread inertia can be considered negligible for the investigated conditions. Calculated time-force records of separation situations including the simple adhesion criterion are similar to experimental results in their character but lack dependence on contact history and unloading rate. The proposed model is able to simulate a tread block indenting and separating from a road surface but the preliminary adhesion model was found to be insufficient and development suggestions are presented.

### **Keywords:**

tyre/road interaction, tyre/road contact modelling, adhesion, non-linear contact stiffness

## Acknowledgements

I am very grateful for the work my supervisor, assistant professor Patrik Andersson, is spending on me and my project, his efforts and company on this journey makes it worth travelling. Professor Wolfgang Kropp is another a key person, I am immensely thankful for his support and knowledge.

I would like to thank the staff and the students at Applied Acoustics for all the encouragement and help, together we make the party! Gunilla Skog and Börje Wijk deserves special attention as they are handling administrative and practical matters in a very impressive way.

Jag vill tacka min familj, mina vänner och Hampus för ert stöd och för att ni, i mina stunder av svårmod, påminner mig om allt det som är roligt med att leva.

# Contents

<b>1</b>	<b>Introduction</b>	<b>1</b>
1.1	Limitations . . . . .	2
<b>2</b>	<b>Background</b>	<b>3</b>
2.1	General background . . . . .	3
2.2	Specific background to this study: small-scale tyre/road contact . . . . .	3
2.3	Road traffic noise and society . . . . .	4
2.4	Tyre/road noise . . . . .	5
2.5	Modelling tyre/road contact . . . . .	8
2.6	Adhesion . . . . .	9
2.7	Tyre/road noise modelling at Applied Acoustics . . . . .	10
<b>3</b>	<b>The new implementation</b>	<b>12</b>
3.1	The general idea . . . . .	12
3.2	Roughness springs . . . . .	14
3.3	Elastic layer . . . . .	17
3.4	How the contact problem is solved . . . . .	20
3.5	Validation of the new implementation . . . . .	25
<b>4</b>	<b>Results</b>	<b>26</b>
4.1	Dynamic calculations - stability problems . . . . .	26
4.2	Means to increase stability . . . . .	28
4.2.1	Increase the time resolution . . . . .	28
4.2.2	Exchange the stiffest roughness springs for softer . . . . .	28
4.2.3	Calculation results - quasi-static conditions . . . . .	29
4.2.4	Calculation results - dynamic calculations . . . . .	30
4.3	Dynamic effects - inertia of the tread . . . . .	32
4.3.1	Linear loading . . . . .	33
4.3.2	Quadratic loading . . . . .	35
<b>5</b>	<b>Introducing Adhesion</b>	<b>38</b>
5.1	The implementation . . . . .	38
5.2	Previous experimental results . . . . .	39
5.3	Brief parameter study . . . . .	40
5.4	Development of the adhesion model . . . . .	43

<b>6</b>	<b>Discussion</b>	<b>46</b>
<b>7</b>	<b>Conclusions</b>	<b>47</b>
<b>8</b>	<b>Future work</b>	<b>48</b>
<b>A</b>	<b>The Newton-Raphson method</b>	<b>51</b>
<b>B</b>	<b>Settings used in the calculations of the elastic layer Green's functions</b>	<b>52</b>
<b>C</b>	<b>Settings and .m-code used in the contact calculations</b>	<b>53</b>
C.1	Dynamic calculations with stability problems . . . . .	53
C.2	Means to increase stability . . . . .	53
C.3	Dynamic effects - inertia of the tread . . . . .	54
C.4	Introducing Adhesion . . . . .	55

## 1 Introduction

Being able to predict and optimise tyres with respect to noise, rolling resistance, grip and wear is an urgent challenge for research. These problems are already today severe in many situations and as traffic is expected to grow substantially over the next years, serious efforts must be taken to minimise the negative effects on people's health and the environment. To accomplish this, accurate and feasible prediction tools are necessary and numerical computer based models have here proven to be of crucial importance.

The context of this study is a numerical tyre/road noise model developed at Applied Acoustic, Chalmers. The key component consists of a contact model predicting the detailed tyre/road interaction and providing the contact forces and how they are distributed in time and space. Including effects of adhesive forces in the contact provides further opportunities for the model.

A numerical time-domain contact model for small-scale tyre tread/road interaction is in this work further developed to investigate the dynamic response of the tread, non-linear contact springs and a primitive adhesion implementation.

### Key questions

- How does the inclusion of inertial effects of the tread affect the contact behaviour? Is a quasi-static approximation sufficiently accurate or must dynamic calculations be made?
- Is the preliminary adhesion model sufficient to reproduce experimental findings?
- When the model is developed, what simplifications can be made?

### Principal results

A numerical model for detailed dynamic tyre/road contact was developed and successfully used when measures to handle numerical instabilities in the calculations were implemented.

Calculation results show that inertia effects of a tread block can be considered insignificant under the investigated conditions.

The simple model that was used to simulate adhesive forces was found to be insufficient and development suggestions are presented.

### Description

The background to this report is the subject of Ch. 2.

How the new implementation is built and how it works is described in Ch. 3.

Calculation results of loading situations are presented in Ch. 4 and of separation situations including adhesive forces in Ch. 5.

The findings of this study are concluded in Ch. 7.

## 1.1 Limitations

The contact model developed in this study is composed by parts previously developed by others. The dynamic response of the tread (modelled as an elastic layer) in the form of Green's functions are as well as the contact springs adapted straight from Andersson [2]. The limitations of these parts due to discretisation in time and space, material uncertainties and numerical implementations are inherited by the present model.

An important limitation of the developed contact model is that only normal contact is studied, tangential motion is not covered but this will be an interesting future extension.

The finite extent of this study led to that questions about possible simplifications are yet to be answered. As the present model works it handles contact on a very small-scale using a very finely resolved scan of a road surface as one of the main inputs. These fine scales are required when studying and gaining knowledge about the detailed contact in a research context but may limit the applicability of the model in an engineering situation.

## 2 Background

This chapter describes in a general manner how this and other studies are needed in the area of tyre/road contact modelling. The specific background to this work is the need for more knowledge about the small-scale tyre/road interaction. The chapter also covers health effects of traffic noise and how this is a growing problem in society. The main tyre/road noise generation mechanisms are then briefly explained and the main parts of the numerical tyre/road noise model at Applied Acoustics are introduced.

### 2.1 General background

The contact between a tyre and the road is of major importance for the overall performance of the vehicle. It also has major implications for the environment and health of people. Fig. 1 is an attempt to summarise the four areas in which tyre/road interaction is important. The interaction of tyre and road essentially determines the tyre/road noise which is the most important contributor to traffic noise in society, at least for higher vehicle speeds. The contact also affects grip and hence both safety and speed capability, rolling resistance and hence fuel consumption and wear of tyre and road which has both environmental and economical aspects. In the following sections it is mainly the noise aspect that will be discussed but the contact model can in principle be use in the other areas as well.

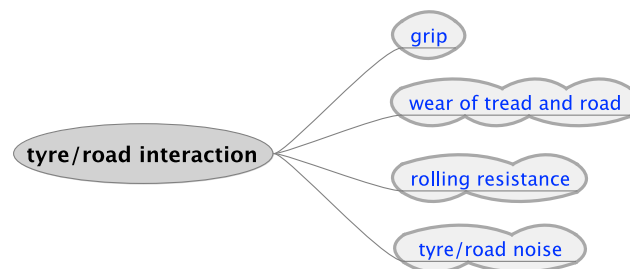


Figure 1: *The contact between tyre and road affects both the safety and health of people as well as the amount of financial means needed for road reparation and tyre re-treading.*

### 2.2 Specific background to this study: small-scale tyre/road contact

The starting-point for this study is the work by Andersson in [1] and [2]. In these references the expression of a non-linear contact stiffness is developed in the context of tyre/road contact modelling. Adhesion is also studied and a model is proposed. But there is a lot left to investigate and develop before these concepts can be incorporated to the contact model and the global tyre/road noise model used at Applied Acoustics (briefly explained in Ch. 2.7).

There is a general need for more understanding about the physics involved in detailed tyre/road contact, the present study is a small step towards increasing knowledge in this area. As one of the specific goals of this work is to increase the capacity of the present tyre/road noise model by also including adhesion and contact-stiffness, there must be developed ways that this can be done in a computationally

feasible manner. An overall aim of this work is hence to find simplification that does not jeopardise the accuracy of the results.

The small-scale roughness of a road surface induces a softer contact between the tyre and the road than if these small-scale variations were missing. In theory a coarser resolution can then be used in the model if the information about the small-scale roughness is collected and transformed into non-linear contact springs. One goal of this work is to incorporate non-linear contact stiffness into a dynamical model. Then questions arise about how these contact springs should look like, how their stiffness should vary with compression? In [2] Andersson used theory for a flat circular punch indenting an elastic layer to get the individual stiffness functions for each contact element. Is it possible to simplify this approach? Could it be possible to use a limited number of stiffness functions? Could they be approximated as linear?

Modelling stick-snap (see Ch. 2.4) requires adhesion to be included in the model. With the approach of contact springs this can be done by adding a force-displacement relation also for elongation of the springs. But how should the adhesion curve look like? Studies show that the strength of the adhesion force is affected by contact time and contact force, how can this be included in the model?

Another question is how detailed the contact patch has to be modelled, how coarse resolution can be used while keeping vital information? The implementation developed in this study uses an embedded rubber tread block of 2x2 cm, same as used in [2]. It is divided into contact elements and the number of elements are 400 (20x20).

Including adhesion and non-linear contact stiffness into a dynamical model was the first goal of this thesis. It has turned out to be very much a question of finding numerical stability and the opportunity of testing different configurations has been limited. The work with investigating parameters and required resolution will continue in the near future but was found to be out of scope for this study.

## 2.3 Road traffic noise and society

Health risks of exposure to noise range from impaired hearing to sleeping disturbances and possible increased risk of cardiovascular diseases. Noise induced hearing loss and other damages like tinnitus are usually caused by very loud sound pressure levels. Community noise from traffic, ventilation, neighbours and industry affects the well-being of people and is a source of increasing annoyance in society.

Sleep disturbances are one of the most severe health risks with environmental noise [3]. Noise makes it more difficult to fall asleep and may affect the depth and continuity of the sleep. During the daytime this may lead to reduced perceived sleep quality, fatigue and decreased performance.

In general, noise can be seen as a stressor with reactions like increased heart rate and stress-hormonal level. The longer the noise exposure the more risk of physiological effects including increased blood pressure and risk of cardiovascular diseases. A recently published study by Selander et al [4] lend some support to the hypothesis that long-term exposure to residential road traffic noise increases the risk of myocardial infarction.

It has been documented that noise adversely affects cognitive task performance but it is not possible to set a guideline value as the effects depend on the type of noise and the task being performed [3]. Direct implications of noise is that it can interfere and mask speech and other important information

communicated with sound. This may lead to a number of stress reactions. Especially vulnerable are people with hearing impairment and people who do not fully master the language.

According to the Swedish National Board of Health and Welfare [5], is noise the environmental disturbance that affects largest number of people in Sweden. It can be assumed that as many as three out of nine millions citizens are exposed to traffic noise levels above the national guidelines. The proportion of people annoyed by noise is increasing and road traffic is the noise source that contributes most to this increase. The number of people annoyed by noise from road traffic at least once a week has increased from approximately 600,000 in 1999 to 800,000 in 2007. The number of people reporting difficulties falling asleep due to traffic noise is also increasing.

The Swedish Institute for Transport and Communications Analysis, SIKA, states a steady increase in road traffic in their report 2005:6 [6]. The forecast for passenger transport gives an increase by 27% between 2001 and 2020 (main scenario, the alternative scenario gives an increase by 17%). Main part of this growth is expected to be car travel. The road transport of goods is expected to increase by 31% for the same period according to the main scenario.

Corresponding forecasts for the European Union are found in [7] (page 62 Table 4.8). In the Baseline scenario, the increase of passenger transport by car (person·km) from 2005 to 2020 is estimated to 20% (35% to year 2030). The increase of freight transport by truck (tonne·km) is expected to be 28% from 2005 to 2020, (43% to year 2030).

## 2.4 Tyre/road noise

The main part of the road traffic noise can be divided in two categories; tyre/road noise and noise generated by the power unit (motor, brakes, exhaust pipes, etc). For average conditions tyre/road noise is dominating at higher speeds (approximately above 40 km/h for passenger cars and 70 km/h for trucks [8]).

An overview of the five main mechanisms connected with tyre/road noise is given in Fig. 2. Contributions from different phenomena can be seen in Fig. 3 that shows calculation results and measured sound pressure level spectrum for tyre/road noise on a road with a rough surface texture [9]. The calculation is made with the noise prediction tool SPERoN [10] for which it is possible to get the contributions from different generation mechanisms. It can be seen that the main radiated noise is in the 1/3-octave bands around 1000 Hz. Tyre vibrations are the dominating mechanism for low and mid frequencies, up to around 1 000 Hz where aerodynamical phenomena start to become more important.

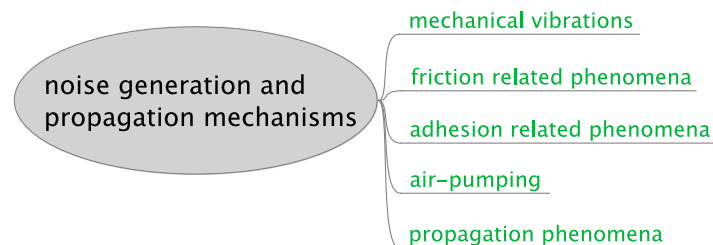


Figure 2: Overview of main tyre/road noise generation mechanisms. Propagation mechanisms are also included in the view.

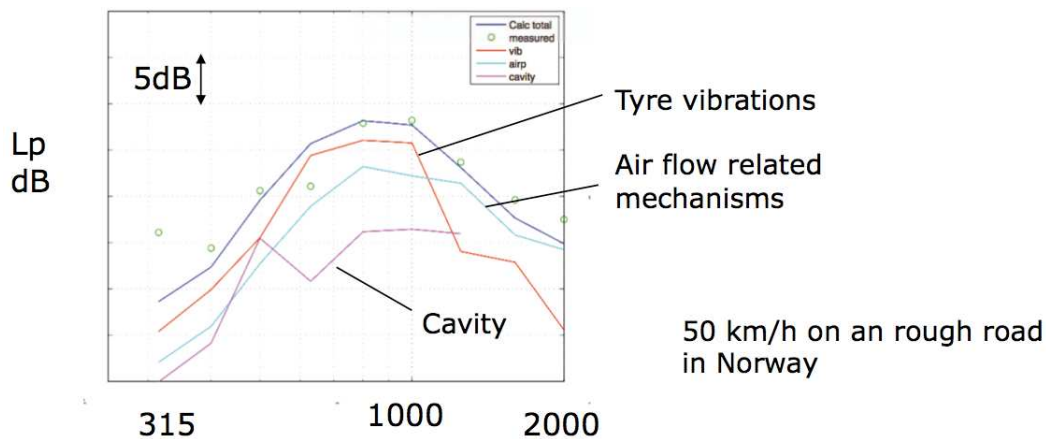


Figure 3: Tyre/road noise spectrum, calculation results from SPERoN [10] and measurements, the figure is taken from [9].

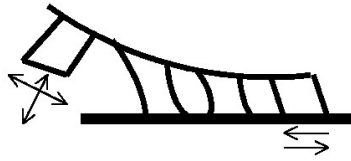
The five important mechanisms connected with tyre/road noise showed in Fig. 1 will now be discussed briefly.

- Mechanical contact forces

A tyre rolling on a road will experience a time-varying radial contact force, small impacts will occur. This excitation force will induce vibrations on the tyre structure which radiate noise. In general will high frequency vibrations rapidly decrease in amplitude when propagating in the tread due to high damping. Low frequency vibrations survive longer, long enough to build modal patterns, and it is believed that tyre vibrations are important for noise generation at low-mid frequencies. Ongoing research is working on finding which of the vibrational modes present on a tyre that are responsible for the main sound radiation [9].

- Frictional contact forces

Friction is a necessary part of the tyre/road contact, it originates both from adhesive effects between the surfaces and from hysteresis as the tread is deformed by the road surface. The presence of friction will give a varying tangential force which will excite tyre vibrations and lead to sound radiation. During rolling, a tyre tread block will stick to the road surface and gradually be deformed by tangential traction forces. The tangential force may well overcome the frictional force that is sticking the block to the road. *Stick-slip*, Fig. 4, is when the tread blocks of the tyre stick and slip relative to the road surface. This usually happens at the trailing part of the contact and constitutes a noise source at the interface in addition to giving extra, tangential force excitation to the global tyre vibrations.

Figure 4: *Stick-slip phenomenon.*

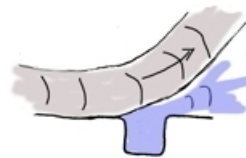
- Adhesive contact forces

*Stick-snap* is an adhesion phenomenon where a force is build up between tread blocks and the road surface, see Fig. 5. When the block is leaving the contact zone it "sticks" to the road until the adhesion force is overcome. Then it "snaps" out of contact, giving an excitation impulse to the tyre and causing as air is rapidly displaced.

Figure 5: *Stick-snap phenomenon.*

- Small-scale aerodynamical phenomenon

The air in and close to the tyre/road contact zone will experience movement, compression and expansion. A number of aerodynamical mechanisms can be distinguished where air-pumping may be one of the most frequently used terms. When the tyre tread enters the contact zone, air is compressed and forced out of the cavities formed by the road and the tread. As it leaves the contact on the trailing edge, air is instead sucked into the contact. This movement causes sound radiation and is called air-pumping, see Fig. 6.

Figure 6: *Air-pumping.*

- Phenomenon related to the propagation

How well the tyre/road noise created in the contact radiates to the surroundings depends on the acoustical radiation impedance. The geometrical shape formed by a tyre and a road resembles a horn. This provides an impedance match for noise generated in the contact zone and this effect may lead to significant amplification of the tyre/road noise, the *horn-effect*. The actual amplification is angle and frequency dependent. It also depends on the road surface, the more

absorbing surface the less horn-effect, and the width of the tyre, the wider the tyre the more horn-effect. Fig. 7 shows how the horn-effect is measured by reciprocity, the loudspeaker is placed in the microphone position and vice versa.



Figure 7: Measurement of the Horn effect using the principle of reciprocity.

The figures, Fig. 5-7, are found on the homepage of the Division of Applied Acoustics, Chalmers University of Technology, [www.ta.chalmers.se](http://www.ta.chalmers.se).

## 2.5 Modelling tyre/road contact

Tyre/road interaction is difficult to model for a number of reasons.

- The contact area is big compared with the wavelength of the vibrations on the tyre. This means that roughness variations in the contact geometry and the dynamical behaviour of the tyre must be considered.
- There are such variety of length-scales involved. From the meter-centimetre-scale of the waviness of the road to the micrometer (or even nanometer) scale of the two meeting surfaces. Taking these small-scales into account in a contact model describing some revolutions of a tyre means tremendous computational effort.
- The contact area and contact pressure will change as function of time, the contact problem is non-linear and must be treated in the time domain. The variation springs not only from the roughness of the road surface but also the tread pattern and low order vibrations on the tyre itself will contribute.
- Adhesive forces are, with varying importance, present in the contact. For certain situations and tyre/road combinations it is crucial to be able to accurately include effects of adhesion.
- The complexity and variety of the tyre structure materials and tread compounds and how their behaviour depend on frequency, strain, temperature, ageing, etc. Data like this are in general very hard to find.

The concept *area of real contact* is important when studying detailed tyre/road contact, and it should be differentiated from the *apparent contact area*. As both surfaces involved in the contact are rough, they only make contact in separate points. The area of real contact is the sum of all these points, or the area associated with them. The estimated area of real contact will hence be a function of the spatial resolution; a coarse resolution will make the contact area appear large, finer resolutions will resolve that not all points within the larger discretisation elements were actually in contact.

Most contact problems consider surfaces with finite stiffness. The area of real contact will then not only depend on the spatial resolution of the geometry but also on the load and material parameters. In the case of an elastic material like the tyre tread, the area of real contact may increase with load

duration time as the material may deform more at asperities with high stress after some relaxation time.

The *apparent contact stiffness* relates the applied load over the apparent contact area to the mean distance between the surfaces (the indentation of the road surface into the tread). In the beginning when just a few points are in contact, an increase of the total load will give a relatively high increase of force per contact point, resulting in a large deformation of the tread at these points. As more and more points come into contact, the share of the applied force at the individual points may decrease and the corresponding deformation of the tread will then also decrease. This means that the *apparent contact stiffness* will increase with indentation for rough surfaces. In addition to this effect, stress-strain relations of the tread are complex with stress-softening and other non-linear effects possibly present.

## 2.6 Adhesion

An adherence force can be defined as the total force needed to separate two surfaces that are sticking to each other due to adhesion at, or in the vicinity of, contact points. These adhesion forces may originate from:

- electromagnetic interaction on the molecular scale
- lower air pressure between the surfaces than in the surroundings
- mechanical interlocking, the two surfaces "hook" on to each other

The electromagnetic interaction believed to be of most importance in tyre/road contact is the weak, long ranged van der Waal force.

The effect on friction of the difference in pressure in the contact region compared to the surroundings is reported by Pinnington in [11] as an "Atmospheric pressure effect". It is believed to be most important for soft rubbers on smooth surfaces when the rubber is lifted rapidly, "The viscous action of the fast moving air seals the gap [...] and the trapped fluid is rarified".

In tyre/road contact it is assumed that mechanical interlocking is of minor importance as such roughness soon would be worn down.

There is an ongoing development of analytical and numerical contact models including adhesion. Heinrich Hertz (1857-1894) is one of the founders of modern contact mechanics, he studied for example the contact of glass lenses pressed together. He developed a theory for the contact of a flat plane and a sphere pressed together assuming smooth, homogeneous, linear elastic materials, no attractive adhesion forces and contact radius much smaller than the radius of the sphere.

Johnson, Kendall and Roberts (JKR) presented in 1971 a contact theory where adhesion was included [12]. One of the factors that led to the development of this theory was that experiments showed that the contact area was larger than predicted by Hertz theory. Adhesion is included at the contact by  $\gamma$  which is the Dupré energy of adhesion or the work of adhesion. It represents the work done in completely separating a unit area of the interface [13]. According to the JKR theory the adherence force during quasi-static conditions is:

$$F_{adh} = \frac{3}{2}\pi\gamma R,$$

where  $R$  is the radius of the sphere.

Deraguin, Muller and Topov derived another theory, DMT, where the contact profile remained Hertzian but where adhesion was accounted for by attractive forces acting where the two surfaces were separated, i.e. around the contact area. In this case the adherence force for a fixed load is:

$$F_{adh} = 2\pi\gamma R,$$

It has been shown that these two theories are good approximations for different types of contacts. The JKR theory works well for softer solids with strong, short ranged adhesion forces and a large sphere radius. DMT works better for the opposite case, hard solids, weaker, more long ranged adhesion and small radius  $R$ . Later, numerical and analytical transitions between the two theories has been developed.

Contact behaviour between rough, non-homogeneous, non-linear elastic surfaces on larger scales is usually difficult to predict and measurements and model updating are common.

## 2.7 Tyre/road noise modelling at Applied Acoustics

The tyre/road noise prediction model at Applied Acoustic (Chalmers University of Technology, Sweden) is divided into three modules as seen in Fig. 8 [9], the contact module, the tyre module and the radiation module.

The contact module is the central part of the tyre/road noise model. Here is the contact geometry and contact forces calculated. The wave field on the tyre is obtained convoluting the contact forces with impulse response functions produced by the tyre module. Aerodynamical noise sources are also calculated in the contact module. The radiation model takes these sources and calculates, together with the geometry and the acoustical impedance of the road, the resulting tyre/road noise.

The tyre/road noise model is continuously undergoing development, more knowledge is gained along the way giving a higher accuracy of the results and making a wider range of situations possible to model. However there is still a lot left to understand and include to achieve a full-developed tyre/road noise model. The tyre model is well developed but better input information is needed, basically this means material data and how the properties of the materials change with circumstances like temperature, frequency, load. Which of the present vibration modes on the tyre that are responsible for most of the sound radiation and how this works is still to be investigated and understood. Input data is also required in the contact module, tread material data, detailed descriptions of road surfaces, friction curves. There is a need to understand more about the detailed contact and how to, in an efficient manner, include effects like non-linear contact stiffness, adhesive forces and tangential forces into the contact model.

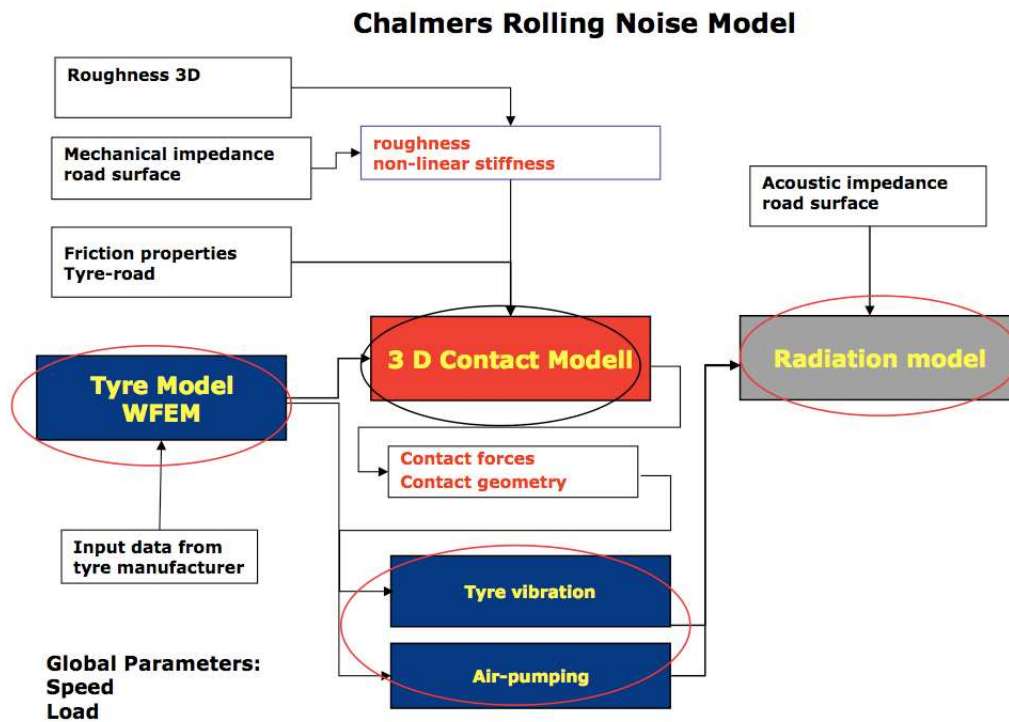


Figure 8: Overview of the tyre/road noise model at Applied Acoustics, Chalmers. The figure is taken from [9].

### 3 The new implementation

This chapter describes the developed tyre/road contact model, how it is build up, the different parts and what restrictions and simplifications that are made. Some effort is also spent on describing how the model is implemented in Matlab.

#### 3.1 The general idea

The model in this work aims at predicting the dynamic contact between a tread block and a road surface. The code is built on the ideas and the model published by Andersson in *Journal of Sound and Vibration* [2], where a more detailed description can be found. The general idea is that a rough road surface is pressed into an elastic layer. The two surfaces are discretised into a grid of *matching points* that potentially can make contact. The problem is solved numerically in the time domain with a Newton-Raphson algorithm and the contact forces and how they develop with time is studied.

In this study concepts like roughness and small-scale roughness of the road surface are important. A high resolution scan of the actual road surface used in the implementation is shown in Fig. 9 [2]. This resolution is in the order of micro meters and it is here referred to as the *small-scale*. The figure also shows how the surface is down-sampled to a 20x20 grid where the height of each element is the height of the outermost point in the corresponding small-scale resolution geometry.

The information about the roughness of the surface that is being lost when using the coarser resolution is taken into account in the model by adding roughness springs between the road and the elastic layer. For each road element there is a corresponding roughness or *contact* spring. When contact is made the term *contact point* is used. It means that a matching point on the elastic layer has met its corresponding outermost point on the road surface. The contact force at this point depends on how much the outer point of the road surface is indenting the elastic layer and the force-compression relation of the individual roughness spring.

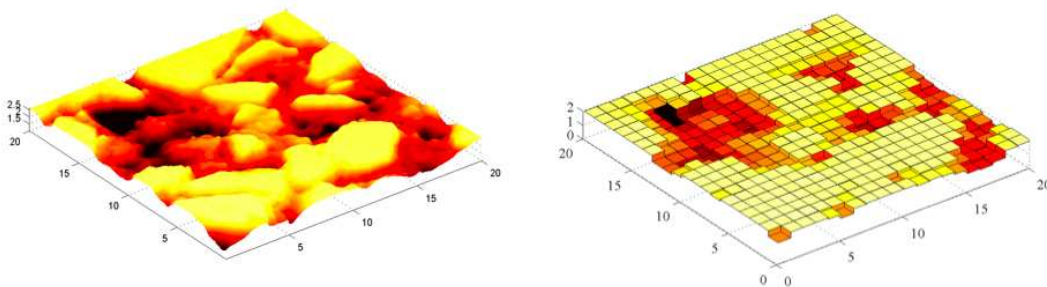


Figure 9: *High resolution scan of the road surface (left) and the same surface but with a coarser resolution of 20x20 elements [2].*

A very brief overview of how the tread and the road are represented in the model and in the implementation can be found in Tab. 1. The problems and restrictions of the model are mainly due to the brute discretisation of an actual continuous problem.

The lowering of the road surface into the elastic layer can be made in various ways. In this work a predetermined indentation has been used. The main advantage with this approach is the controllability with respect to loading rate and load duration.

The roughness springs are considered as non-inertial and hence they do not have an impulse response lasting over time. Instead they are taken into account by two functions, one that gives the stiffness as a function of compression and one that gives the spring force as a function of compression. The spring force function is the primitive function of the spring stiffness function and hence differentiating the spring force function with respect to compression gives the stiffness function. In the case of linear roughness springs these are simple functions, a constant and a straight line. But when estimating them from a real road surface, they become non-linear with much lower spring stiffness for small compressions than for large. The non-linearity of these springs are stressed by the use of a spiral spring symbol, see Fig. 16.

The elastic layer is represented by Green's functions. In addition to giving the impulse response at the point of excitation they also contain information about what is happening at the other points. The response in one point will be a superposition of the response from each excitation point. The displacement of the elastic layer is obtained by convolution of the roughness spring force in each contact point with the elastic layer Green's functions.

To solve the contact problem and find the compressions of the roughness springs and the displacement of the elastic layer, a function is defined so that it is equal to zero for the "true" compression of the roughness springs. Then this point is sought in a Newton-Raphson iteration where what is happening in the present time step also is influenced by what has happened before by the Green's functions involved. When the solution is below an error limit, the final displacements and forces are calculated for the present time step and future displacements due to these are stored. Then the next time step is started with a new displacement of the mass-spring system and hence new compressions of the roughness springs and the elastic layer will have to be sought.

Table 1: A brief overview of how the contact situation is modelled and how this model is implemented.

Real thing	In the model thought of as	In the implementation
Tread	An elastic layer attached to a rigid backing	A set of Green's functions
Road	A set of roughness springs to account for the small-scale roughness	Individual roughness spring functions describing the spring stiffness and spring force as a function of compression
	A 2x2 cm infinitely stiff body with a discretised surface geometry that neglects small-scale roughness	A set of numbers that represents the height of these different surface elements

### 3.2 Roughness springs

Virtual springs are added in the contact between the block and the road surface to compensate for the coarse resolution used in the implementation. A higher resolution is not computationally feasible and using a coarse resolution of the contact patch without them would mean either full contact or no contact at all - an approach far from reality.

The apparent stiffness of rubber depends on the excitation area, the larger the contact area the stiffer the contact. This gives an idea of why the roughness springs are needed, when a contact element reaches the elastic layer it is actually only the outermost point that first makes contact, see Fig. 10 [1]. The elastic layer will deform more easily for this small area indentation. As the element is lowered further, more and more points within the element will make contact and the elastic layer will not deform as easily as before. By adding roughness springs the points representing the small-scale roughness within one element is modelled without the spatial resolution else needed.



Figure 10: An elastic layer that is pressed down into a road surface with small-scale roughness will experience an increasing stiffness as more and more small-scale points make contact, i.e. as the contact area increases [1].

The non-linear roughness springs used in this study are directly adapted from Andersson [2]. The end points of the stiffness functions are to some extent intuitive, before the two bodies make contact, i.e. before the outermost point on the road meets the elastic layer, the stiffness should be zero. When fully indented, all small-scale points are in contact and the interfacial stiffness should be infinite. This means that there will be no compression of the roughness springs and the contact force will directly reach the bulk of the elastic layer. For the the stiffness function to work in a Newton-Raphson algorithm there is a requirement that it must be analytical and differentiable. There is also a wish for the function to be monotonically increasing for increasing compression of the spring. This stems partly from the question of uniqueness and partly because the opposite must be seen as non-physical.

The compression relations of the roughness springs, stiffness and force as a function of compression, can be found from a high resolution scan of the road surface by studying the area of contact as a function of depth (indentation). This is done for each element of size given by the wanted resolution. An approach suggested by Yang [14] gives the resistive force in the case of a flat circular punch indenting an elastic layer with a finite thickness. The force in the small-scale roughness spring can hence be determined when the area of contact for each indentation step is translated to an equivalent circular punch. Fig. 11 [2] shows a 2D example of a high resolution scan of a road element. The outermost and the lowest points are labelled  $z_{max}$  and  $z_{min}$ . Indentation,  $\delta$ , is here formulated as being positive when below  $z_{max}$ . The thickness of the elastic layer in Yang's method is chosen to be the height,  $h(\delta)$ , between the current indentation and the lowest point. In this way the roughness springs will get stiffer for deeper indentations.

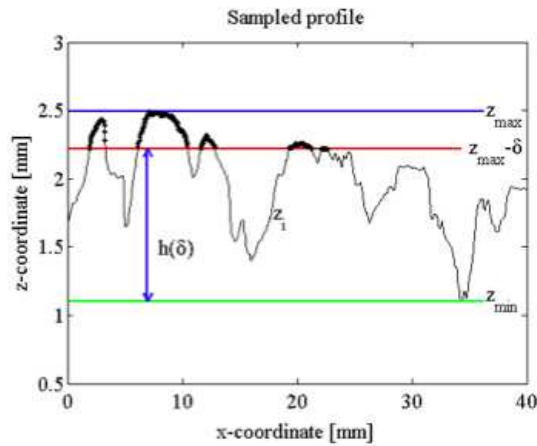


Figure 11: The high resolution scan of a road element is the starting point when building an individual roughness spring. The outermost and the lowest points are labelled  $z_{max}$  and  $z_{min}$ . The stiffness/spring force is evaluated for every indentation step,  $\delta$ . Figure is taken from [2].

The roughness spring force functions used in this study, originally created and tested by Andersson [2], were found by applying a polynomial approximation to the results from Yang's formulas. The stiffness functions were found by taking the derivative of the spring force functions. Examples of stiffness functions and spring force functions can be seen in Fig. 12. The present stiffness functions can be considered as first versions of future, adapted and optimised versions.

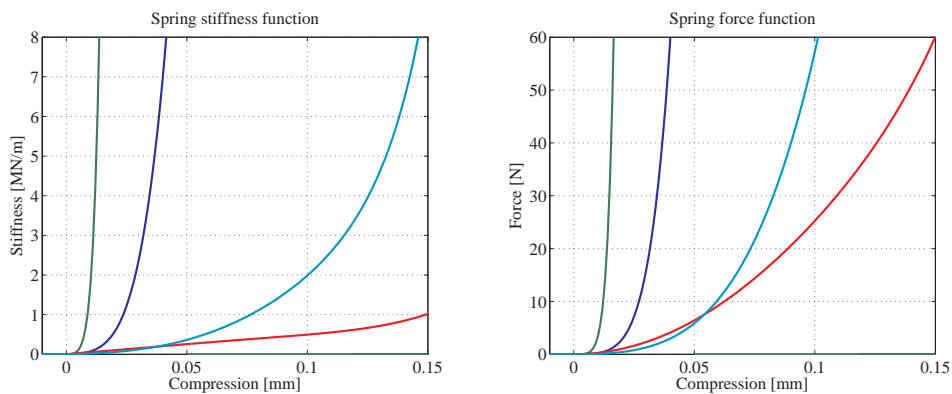


Figure 12: Spring force functions and their corresponding stiffness functions for four elements.

### Discussion about the formulation of the roughness springs

One of the assumptions built into the roughness spring relations is the fact that the elastic layer used in Yang's method is considered to be without inertia. Hence the roughness springs are without inertia and they respond immediately to a compression. This is though not expected to impose any significant errors on the results since this elastic layer is relatively very thin.

The radius of the punch is deducted from the sum of the areas associated with all small-scale points situated above the current indentation, recall Fig. 11. This is a major simplification and at the present stage it is not completely clear how much the resulting roughness spring relations are effected.

The incompressible characteristics of the elastic layer will make the resistive force depend on the thickness of the layer in relation to the area of the indentation. Gathering all indenting areas within one element into a circular punch might, for small indentations where the elastic layer is more similar to an elastic half space, underestimate the stiffness. For larger indentations where thin layer theories are applicable to the elastic layer, it is the other way around, the stiffness may be overestimated. Currently ongoing investigations will bring more clarity into uncertainties of this kind concerning the approximations done when estimating the roughness spring relations.

The resolution of the roughness springs is limited by the resolution of the small-scale roughness of the road, i.e. the resolution of the laser scan. The limited resolution will cause discrete jumps in the output from Yang's model and the stiffness functions may not fulfil the requirements of being monotonically increasing, analytical and differentiable. To overcome these problems a polynomial fit of order ten is applied to the results with a restriction that the derivative must be positive. The deviation between the polynomial approximation and the original results are more pronounced for small indentations.

The approach to increase the accuracy and feasibility of the contact model by the aid of roughness springs is relatively new and effort must be taken to investigate their importance and how detailed they must be described. When implementing them questions arise about what, if any, simplifications that can be employed and the errors they induce; What is the spatial resolution needed, is it possible to just use a set of "standard" stiffness functions, is it possible to use linear approximations? Answers to these questions may also provide guidance whether the present method to build roughness springs is accurate enough or if greater care has to be taken with the under/overestimation of stiffness for example.

### **Adhesion conditions implemented in the roughness springs**

In this work attempts are made to include a simple adhesion model in the contact calculations. In practice this is done by making the spring stiffness and force functions also work for elongation. It should be clearly stated that the adhesion model in the present implementation is merely a test and the values on the parameters are to some extent arbitrary. Fig. 13 shows examples of roughness spring stiffness and force functions with the simple type of adhesion criterion used in this work. For compressions the spring works as described previously but here it also gives a mirrored force of opposite sign when the compression is negative, i.e. when the spring is elongated. The figure describes a snap-off behaviour, the adhesion can only hold for a certain amount of force, a *release criterion*, when it is exceeded the contact is lost. This type of spring force function also describes a snap-on effect that will make the bodies being sucked towards each other before the outermost small-scale point on the road surface make contact with the elastic layer. Even though snap-on effects exists for contacts on the nanometer scale, see for example [15], it is not considered in this model. The problem is circumvented by an evaluation in each time step of which points that are in contact with the elastic layer, the others are excluded from the present Newton-Raphson iteration.

Future developments of the implementation will take the contact on smaller length scales into account. It will also include an adhesion force that varies with load, load duration and separation speed. One example that could be investigated is the semi-empirical model suggested by Andersson and Kropp in [16].

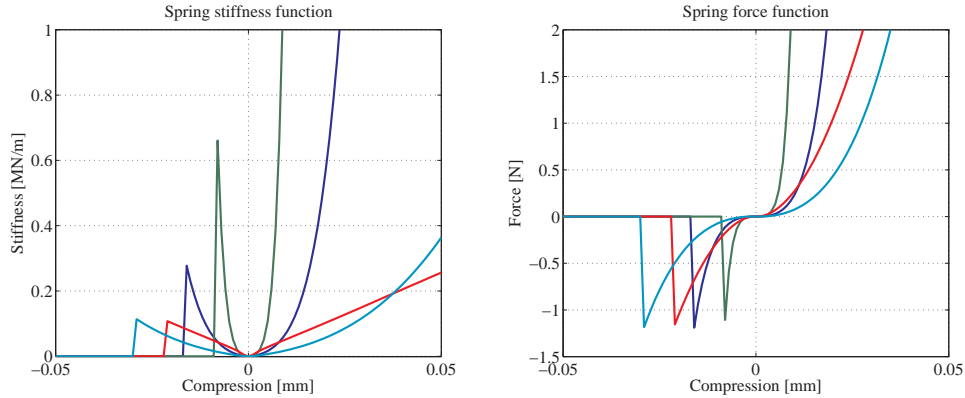


Figure 13: *Spring force functions with adhesion properties. Adhesion is here modelled as the mirror of the positive force-indentation relation together with a release criterion; a maximum separation force for which the contact will break.*

### 3.3 Elastic layer

The elastic layer representing the tread is in this study modelled by a modified version of the two-layered elastic plate model by Larsson and Kropp [17]. The fundamentals of the original model are described in this chapter as well as the modifications and the resulting elastic layer Green's functions used in the present work.

In this implementation the elastic layer is modelled by a 1x1 meter wide, 1.3 centimetre thick, double layered elastic plate with a perfectly rigid backing. The plate is simply supported along its edges and no external tension is present. The two layers are continuously coupled so that pressure and displacement in all directions are equal at the interface. The displacement response given by the Green's functions is the response in the normal direction at the surface of the top layer. More detailed information about the parameters used when creating the elastic layer Green's functions can be found in Appendix B.

The original model by Larsson and Kropp [17] starts in the time domain by setting up the general field equations, Eq. 1, for an elastic plate. Here the plate represents an unfolded and flattened tyre with one layer being the softer rubber tread and the second being the stiffer belt. The plate is under external tension and the boundary conditions are set to simply supported along the rim edges and periodic in the circumferential direction.

The general field equations, Eq. 1, that governs the motion of an elastic plate can be derived by studying the potential and kinetic energy and applying Hamilton's principle. Solutions to these equations, i.e. wave types and dispersion relations, can be found by a transformation into the frequency-wave number domain accompanied by applying simplifications, boundary conditions and matrix algebra. The resulting frequency response functions are then transformed back into the time domain by an inverse Fourier transform method.

Hamilton's principle is an important part of Lagrangian mechanics. It states that the true dynamics of a system between two known states at time  $t_1$  and  $t_2$  will be such that the variational integral of

the Lagrangian is an extreme point. By calculating the variation according to Hamilton's principle the general field equations, GFE, can be derived, here with an external tension in the x-direction:

$$\begin{aligned} G \left[ \Delta u_x + \frac{1}{1-2\nu} \frac{\partial}{\partial x} \nabla \mathbf{u} \right] + \sigma_0 \frac{\partial^2 u_x}{\partial x^2} &= \rho \frac{\partial^2 u_x}{\partial t^2} \\ G \left[ \Delta u_y + \frac{1}{1-2\nu} \frac{\partial}{\partial y} \nabla \mathbf{u} \right] + \sigma_0 \frac{\partial^2 u_y}{\partial x^2} &= \rho \frac{\partial^2 u_y}{\partial t^2} \\ G \left[ \Delta u_z + \frac{1}{1-2\nu} \frac{\partial}{\partial z} \nabla \mathbf{u} \right] + \sigma_0 \frac{\partial^2 u_z}{\partial x^2} &= \rho \frac{\partial^2 u_z}{\partial t^2} \end{aligned} \quad (1)$$

, where  $\mathbf{u}(x, y, z, t)$  is the displacement vector,  $G$  is the shear modulus,  $\nu$  is Poisson's ratio and  $\sigma_0$  an external tension.

Exciting the elastic layer with a harmonic force (i.e. studying the response for one excitation frequency at a time) will result in a stationary amplitude wave field. In analogy to a time-amplitude signal that can be decomposed into its frequency components, this field can be described as sum of waves with different wave numbers. The unknown displacements in Eq. 1, are found by first transforming them from the time-space domain to the frequency-wave number domain. In this domain the variables consists of the triple integral over all wave numbers in the three directions and the corresponding unknown weights. For example the displacement in x-direction can be written:

$$u_x = \frac{1}{(2\pi)^3} \iiint_{-\infty}^{\infty} \hat{u}_x(k_x, k_y, k_z) e^{-jk_x x} e^{-jk_y y} e^{-jk_z z} e^{j\omega t} dk_x dk_y dk_z \quad (2)$$

By inserting this and the corresponding expressions for  $u_y$  and  $u_z$  into the GFE, the problem is turned into an algebraic equation system (inside the triple integral). The mobility of the elastic layer is found by studying this equation system with a wave approach. From the resulting frequency response function, the impulse response in the time-space domain can be calculated by an inverse fourier transformation. To reduce problems such as ripples due to Gibbs phenomenon and non-causality and to ensure the right step response, the "Two-times the real part"-method is used. More information about this method can be found in the PhD thesis of Andersson [1].

The resulting Green's functions contain information about the responses in all elements due to a unit force impulse applied in one point. The responses at time step  $k$ ,  $\mathbf{g}_{el}(k)$ , can hence be written as a matrix:

$$\mathbf{g}_{el}(k) = \begin{bmatrix} \mathbf{g}_{1 \rightarrow 1}(k) & \mathbf{g}_{2 \rightarrow 1}(k) & \dots & \mathbf{g}_{M \rightarrow 1}(k) \\ \mathbf{g}_{1 \rightarrow 2}(k) & & & \vdots \\ \vdots & & \ddots & \\ \mathbf{g}_{1 \rightarrow M}(k) & \dots & & \mathbf{g}_{M \rightarrow M}(k) \end{bmatrix}, \quad (3)$$

where  $M$  is the total number of elements and  $\mathbf{g}_{i \rightarrow j}(k)$  denotes the response in element  $j$  due to a force in element  $i$ , at time step  $k = \{0, 1, \dots, Q-1\}$  after the excitation, where  $Q$  is the number of samples in the Green's functions.

The Green's functions used in this work are 256 samples long with the same sampling frequency that is used in the contact algorithm, 51.2 kHz. Fig. 14 shows how the contact patch is divided into, in this case, 10x10 elements and how there are Green's functions describing what happens in each element due to an excitation in point 1. When the excitation occurs in another element, symmetry is used to find the corresponding Green's functions for the responses in all the other points, hence not all elements in Eq. 3.4 are necessary.

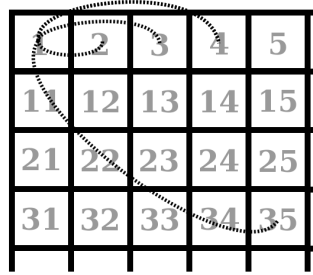


Figure 14: Elastic layer contact patch divided into 10x10 elements, each having a Green's function describing the response due to an excitation in element 1.

Examples of elastic layer Green's functions can be seen in Fig. 15 where the first 13 time samples are shown. The contact patch is here divided into the default number of elements, 20x20.

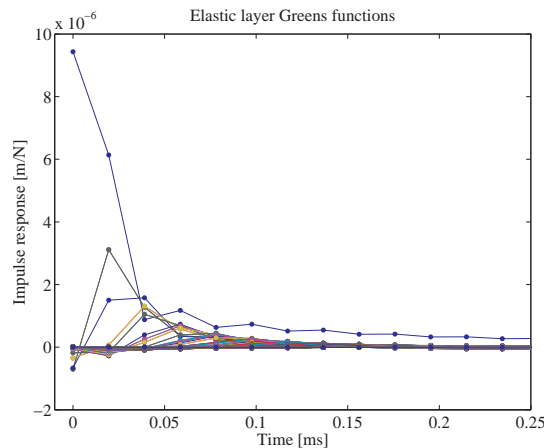


Figure 15: The first 13 time samples of the Green's functions of the elastic layer.

A common approach is to approximate the system as quasi-static. This means that the time response of the elastic layer is allowed to wear off before something new happens. What remains of the Green's functions is the last value of the step response, i.e. the final displacement when the system has settled after a unit step force is applied. In practice this done by summing the values in the Green's function, taken into account the time resolution.

Modelling the contact in discrete time steps has inherent problems and when studying the Green's functions of the elastic layer there are some main concerns. The limited time resolution of the func-

tions stems from the fact that there is a practical frequency resolution and an upper frequency limit, where it is feasible to solve the general field equations. The large jump in amplitude between the first and the last sample of the Green's functions is troublesome to resemble, even with an infinite number of frequencies, and the Gibbs phenomenon will give ripples in the impulse responses. "Two-times the real part method" improves the performance of the inverse Fourier transformation when building the Green's functions, but it has a strong requirement of sufficient damping and may not work beneficially in all cases. Material data and deficiencies in how the damping is modelled are other important sources of uncertainties.

A last remark is to make an attempt to clarify the usage of "Green's function" in this report. Green's functions are in general defined as the response when the excitation is a perfect Dirac delta pulse, due to our frequency limitations this is not strictly fulfilled. Hence what is referred to as Green's functions in this work should be considered as impulse response functions with limited time resolution.

### 3.4 How the contact problem is solved

The contact model in this work is build upon the model and ideas of Andersson presented in [2]. It works in the time domain and a solution is found for each time step by performing a Newton-Raphson iteration, but only for the points that are actually in contact. This section describes how the contact problem is formulated and solved in a matlab implementation. It also covers the necessary input of the model and the possible output.

During the contact calculation two bodies, the elastic layer and the road surface, are gradually making contact. More and more contact points enter the algorithm where the main goal is to find the contact forces and the distribution and development of these. The variables involved are the compressions of the roughness springs, the displacement of the elastic layer and the vertical positions of the road elements. The total number of elements is here denoted  $M$ , and the number of elements in contact  $P$ .

The concept of the model and the how the variables are defined is showed in Fig. 16. The figure demonstrates a system where the whole contact patch is discretised into one element. The same definitions hold in a multi-point system and variables that have a value for each discretisation point will in the following be marked with bold letters.

The position of the road is given by the variable  $d_{\text{road}}(n)$  where  $n$  is the present time step. The initial distance between the road and the elastic layer is given by  $z_{\text{free}}$ . The outermost heights of the matching points on the road are given by the vector  $\mathbf{z}_{\text{road}} = (z_{\text{road } 1}, z_{\text{road } 2}, \dots, z_{\text{road } M})^T$ .

As the elastic layer is forced into the road, this indention will be divided between displacement of the elastic layer,  $\mathbf{d}_{\text{el}}(n) = (d_{\text{el } 1}(n), d_{\text{el } 2}(n), \dots, d_{\text{el } M}(n))^T$ , and compression of the roughness springs,  $\mathbf{d}_{\text{rs}}(n) = (d_{\text{rs } 1}(n), d_{\text{rs } 2}(n), \dots, d_{\text{rs } P}(n))^T$ . When they are compressed they transmit a roughness spring force, a contact force, to the elastic layer which responds to this force according to its Green's functions.

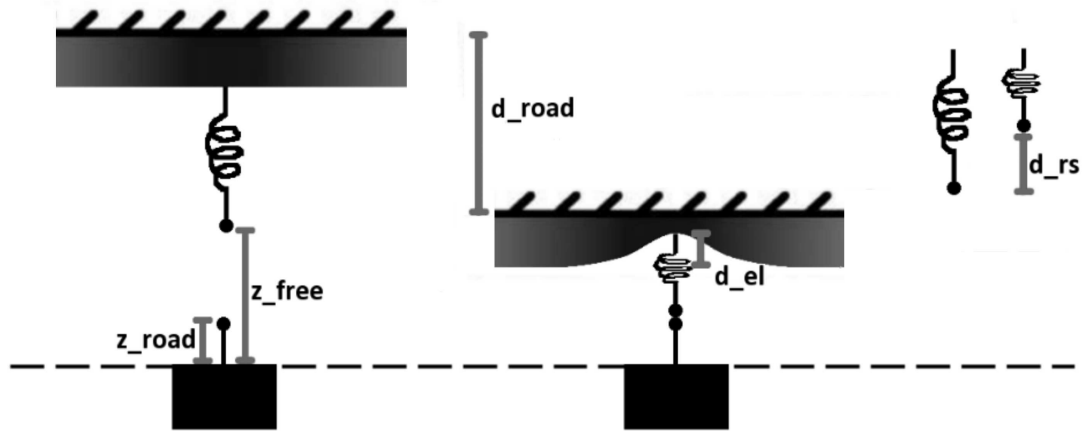


Figure 16: The concept and variables of the contact model, initially (left) and at an instant time step (time index  $n$  is left out) (right). The position of the road is given by the variable  $d_{road}$ . The outermost heights of the matching points on the road are given by  $z_{road}$  and the initial distance between the road and the elastic layer is given by  $z_{free}$ . The displacements of the elastic layer is given by  $d_{el}$  and the compressions of the roughness springs by  $d_{rs}$ .

In the calculations, the predetermined indentation of the road into the elastic layer,  $d_{road}(n)$ , enters each time step as a constant.

The compressions of the roughness springs,  $d_{rs}(n)$ , are used as arguments to get the spring forces,  $\mathbf{F}_{rs}(d_{rs}(n)) = [F_{rs1}(d_{rs1}(n)), F_{rs2}(d_{rs2}(n)), \dots, F_{rsP}(d_{rsP}(n))]^T$ , and the spring stiffness values  $\mathbf{k}_{rs}(d_{rs}(n)) = [k_{rs1}(d_{rs1}(n)), k_{rs2}(d_{rs2}(n)), \dots, k_{rsP}(d_{rsP}(n))]^T$ , of the present time step. More information about these relations are found in Ch. 3.2.

The displacements of the elastic layer,  $d_{el}(n)$ , are calculated by convolution of the forces from the roughness springs,  $\mathbf{F}_{rs}(d_{rs}(n))$ , with the Green's functions of the elastic layer, including the time step size  $\Delta t$ . The convolution is in practise divided in two parts, one which handles the responses due to forces in the present time step, and one where the responses in future time steps are calculated. The first part is given by multiplication of the forces in the present time step with the first values in the Green's functions,  $\mathbf{g}_{el}(0)$ , representing the instant impulse responses. The responses in future time steps due to forces in the present, are calculated after a solution to the Newton-Raphson iteration has been found for the present time step. The determined contact forces are then used in a discrete convolution with the complete Green's functions of the elastic layer.

The displacement of one elastic layer element  $m = \{1, \dots, M\}$ , in the present time step  $n$ , can hence be expressed as the sum of the responses due to the forces in all present contact points  $p = \{1, \dots, P\}$ , plus the response due to forces in previous time steps:

$$d_{el m}(n) = \sum_{p=1}^P F_{rs p}(d_{rs p}(n)) \cdot \mathbf{g}_{el p \rightarrow m}(0) \cdot \Delta t + d_{el old m}(n), \quad (4)$$

where

$$\mathbf{d}_{\text{el old } m}(n) = \sum_{k=0}^{n-1} \sum_{p=1}^P \mathbf{F}_{\text{rs } p}(\mathbf{d}_{\text{rs } p}(k)) \cdot \mathbf{g}_{\text{el } p \rightarrow m}(n-k) \cdot \Delta t \quad (5)$$

The compressions of the roughness springs are determined numerically in a Newton-Raphson iteration. For this purpose a function is defined,  $\mathbf{f}(\mathbf{d}_{\text{rs}}(n)) = [f_1(\mathbf{d}_{\text{rs}}(n)), f_2(\mathbf{d}_{\text{rs}}(n)), \dots, f_P(\mathbf{d}_{\text{rs}}(n))]^T$ , that is zero for the sought  $\mathbf{d}_{\text{rs}}(n)$  of the present time step. A brief explanation of the Newton-Raphson method can be found in Appendix A. The Newton-Raphson function can be written:

$$\mathbf{f}(\mathbf{d}_{\text{rs}}(n)) = \mathbf{d}_{\text{road}}(n) + \mathbf{z}_{\text{road}} - z_{\text{free}} - \mathbf{d}_{\text{el}}(n) - \mathbf{d}_{\text{rs}}(n) \quad (6)$$

The system is now defined to have as many Newton-Raphson functions as points in contact,  $P$ . The next step is to differentiate these functions with respect to the compressions of the roughness springs,  $\mathbf{d}_{\text{rs}}(n)$ . The only variable in Eq. 6 that is dependent on these compressions, except  $\mathbf{d}_{\text{rs}}(n)$  itself, is the displacements of the elastic layer  $\mathbf{d}_{\text{el}}(n)$ . This will result in the derivative of the roughness spring force with respect to the compressions of the roughness springs, times the first value in the Green's functions. This derivative is, as mentioned in Ch. 3.2, equal to the roughness spring stiffness function.

The differentiation of each Newton-Raphson function must be done with respect to each individual roughness spring and the result is a *functional matrix*,  $\mathbf{f}'(\mathbf{d}_{\text{rs}}(n))$  of size  $P \times P$ :

$$\mathbf{f}'(\mathbf{d}_{\text{rs}}(n)) = \frac{\partial \mathbf{f}(\mathbf{d}_{\text{rs}}(n))}{\partial \mathbf{d}_{\text{rs}}(n)} = \begin{bmatrix} \frac{\partial f_1(\mathbf{d}_{\text{rs}}(n))}{\partial d_{\text{rs } 1}(n)} & \frac{\partial f_1(\mathbf{d}_{\text{rs}}(n))}{\partial d_{\text{rs } 2}(n)} & \dots & \frac{\partial f_1(\mathbf{d}_{\text{rs}}(n))}{\partial d_{\text{rs } P}(n)} \\ \frac{\partial f_2(\mathbf{d}_{\text{rs}}(n))}{\partial d_{\text{rs } 1}(n)} & \ddots & & \vdots \\ \vdots & & & \\ \frac{\partial f_P(\mathbf{d}_{\text{rs}}(n))}{\partial d_{\text{rs } 1}(n)} & \dots & & \frac{\partial f_P(\mathbf{d}_{\text{rs}}(n))}{\partial d_{\text{rs } P}(n)} \end{bmatrix} \quad (7)$$

The expressions for the Newton-Raphson function and an element in the functional matrix can now be written:

$$\begin{aligned} \mathbf{f}(\mathbf{d}_{\text{rs}}(n)) &= d_{\text{road}}(n) + \mathbf{z}_{\text{road}} - z_{\text{free}} \\ &\quad - \mathbf{g}_{\text{el}}(0) \cdot \mathbf{F}_{\text{rs}}(\mathbf{d}_{\text{rs}}(n)) \cdot \Delta t + \mathbf{d}_{\text{el old}}(n) \\ &\quad - \mathbf{d}_{\text{rs}}(n) \end{aligned} \quad (8)$$

$$f'_{i,j}(\mathbf{d}_{\text{rs}}(n)) = -\mathbf{k}_{\text{rs } i}(\mathbf{d}_{\text{rs } i}(n)) \cdot \mathbf{g}_{j \rightarrow i}(0) - \delta_{ij},$$

where  $\delta_{ij}$  is the Kronecker delta.

Input to the model is information about the two bodies that meet, the road and the elastic layer. Detailed data of the geometry of the road is important for the construction of the roughness springs and the information about the outermost height that enters the implementation with the  $\mathbf{z}_{\text{road}}$  variable. When constructing the Green's functions for the elastic layer the material data is crucial. It is usually very difficult to obtain this data, especially in the view of the softening of the rubber the smaller the excitation area and damping.

The present output from the contact calculations are the time dependent displacements of the elastic layer and the compression of the roughness springs giving a contact force for each contact point. The

results are in general presented by the total contact force as a function of indentation, the resulting contact stiffness is then obtained by differentiating this contact force with respect to indentation. When plotting differences between curves which are given at different indentation points, the matlab interpolation function `interp1(linear)` is used. Results will also be presented by plotting the contact stiffness as a function of contact force.

The model has been implemented in Matlab which has the main advantage of providing relatively easy ways to obtain graphical results. In future implementation parts of the code could be written in a faster language and be coupled to the main matlab code. The main steps in the code are shown in the code map, Fig. 17.

The code starts with defining parameters and loading the surface data of the road. Then the parameters for the roughness springs, the elastic layer and the road are defined and the actual contact calculation part start. For each time step the number of points in contact is checked. When there is at least one point in contact the Newton-Raphson iteration starts (abbreviated NR in Fig. 17). The iteration is only done for the points in contact but for the next Newton-Raphson step there is an evaluation if more points should be included in the contact. The iteration continues until all  $\mathbf{d}_{rs}(n)$  are found that gives a smaller value of the Newton-Raphson functions than a pre-determined error limit,  $|\mathbf{f}(\mathbf{d}_{rs}(n))| < \text{error limit}$ . Before the next time step the future displacements of the elastic layer due to the forces in this time step are calculated and stored in the  $\mathbf{d}_{elold}$  variable with arguments for the future time steps  $(n + 1, n + 2, \dots)$ .

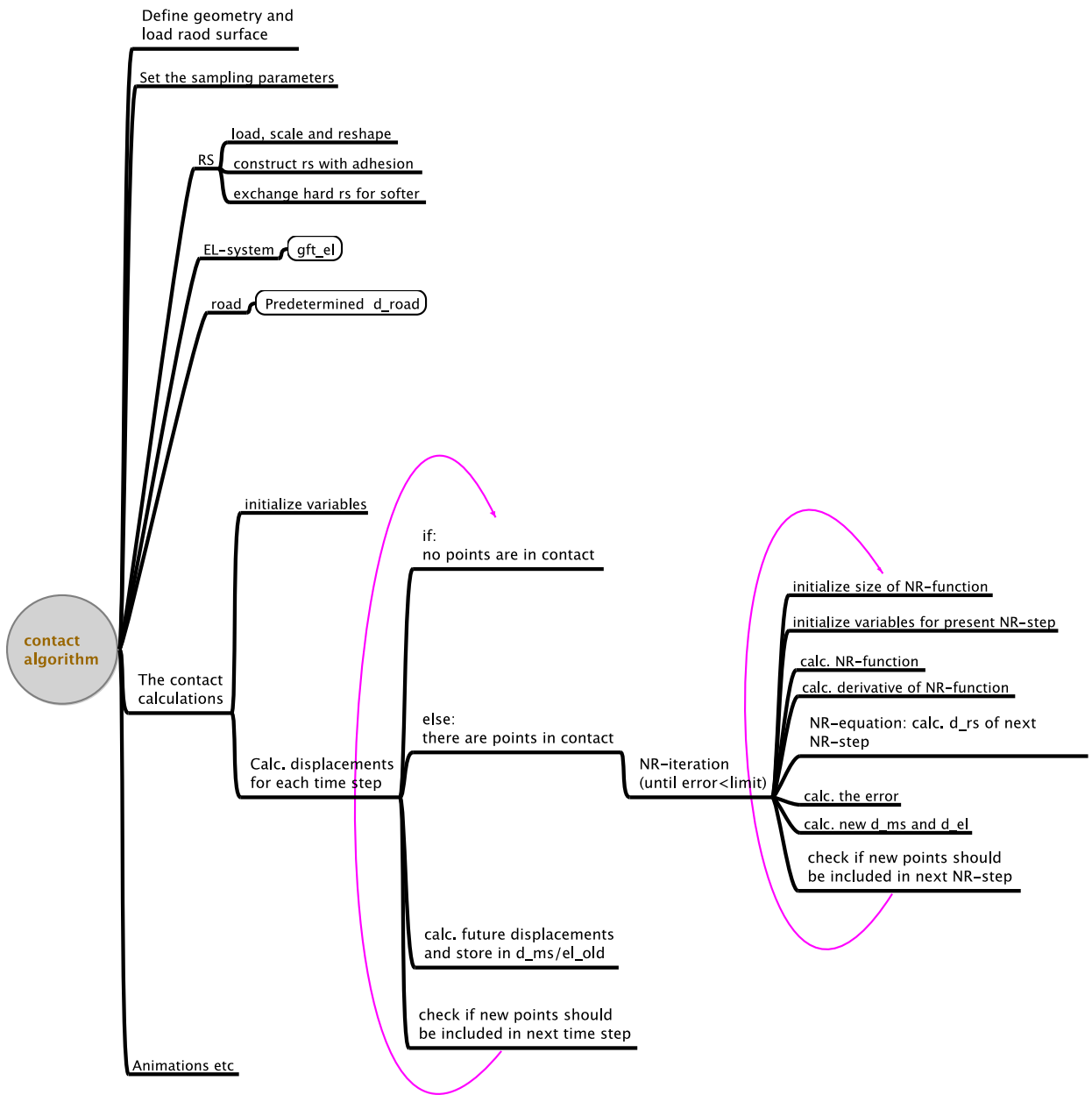


Figure 17: A map over how the model's matlab code work (created with FreeMind). The iterative steps are marked with arrows.

### 3.5 Validation of the new implementation

The contact force-indentation record of the new implementation is compared with the result of Andersson in [2] for the same tread parameters and the same road surface geometry. Quasi-static conditions are assumed in both calculations and Fig. 18 shows that they give the same results. It is concluded that the model works as expected.

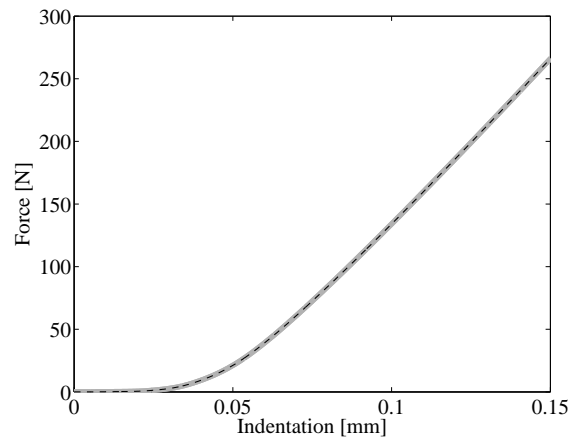


Figure 18: Contact force as a function of indentation for quasi-static case, Andersson's implementation (thick grey line) [2], present implementation (dashed black line).

## 4 Results

The contact model as presented in the previous chapter is here investigated. It manages quasi-static situations well but stability problems arise when solving dynamic problems. Two different means to increase stability are tested with positive outcomes, stability is increased and the results are not altered to any greater extent. At this point the difference between dynamic and quasi-static calculations can be studied. It is concluded that the inertia of the tread seems to be of minor importance; quasi-static conditions may be a very good approximation.

### 4.1 Dynamic calculations - stability problems

The dynamic calculations of the a tread block indenting a road surface manage up to a certain point where instabilities takes over and the results no longer make sense. It is a complex system and in this chapter the instability is tested by increasing the number of Newton-Raphson iterations, different/better initialisation of the Newton-Raphson variable. Different loading rates of the predetermined indentation are also tested. It seems like non of these actions change the instability to any noticable extent. Details about the calculation can be found in Appendix C.1.

The indentation limit for the present block and road surface is around 0.06 millimetre as can be seen in Fig. 19. The figure shows the contact force (left) and the number of required Newton-Raphson iterations (right) as a function of indentation for dynamic and quasi-static conditions. It is clear that the dynamic results are erroneous after the limit, the number of required iterations in each time step suddenly reach the maximum ten and the contact force starts to oscillate and then shoot up to extreme values. Allowing for more Newton-Raphson iterations does not change the situation, the algorithm can not find the right values of the compression variable to make the system stable.

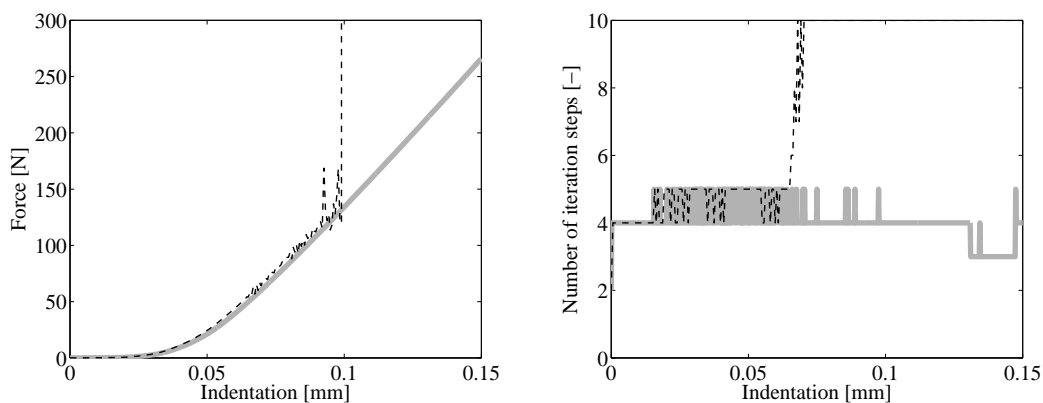


Figure 19: *Contact force (left) and number of required Newton-Raphson iterations (right) as a function of indentation for dynamic (dashed) and quasi-static conditions (thick grey).*

The Newton-Raphson algorithm is sensitive to the initialisation of the variable to solve. In Fig. 19 the compression variable of the roughness springs was in each new time step initialised to the final value of the last time step. A more refined guess is to chose it from a linear interpolation of the final values

of the last and the second last time steps. The result of this approach is shown in Fig. 20, it can be concluded that the refined initialisation did not affect the instability to any greater extent.

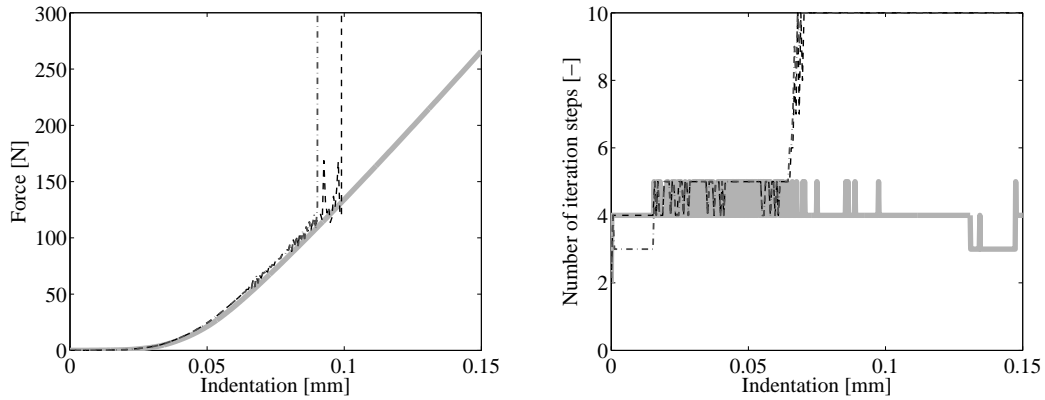


Figure 20: Contact force (left) and number of required Newton-Raphson iterations (right) as a function of indentation for dynamic conditions with original (dashed) and refined (dash-dotted) initialisation, quasi-static conditions (thick grey).

As the quasi-static case is free from instabilities one idea is to approach a quasi-static situation by using a slower indentation rate, using a faster should in this case give worse stability problems. So far a linear predetermined indentation with a rate of 0 to 0.2 mm in 6.7 ms have been used, displayed in Fig. 30 with triangular markers. Fig. 21 shows the results of the dynamical calculation when using this and the other indentation rates in Fig. 30. The results shows no improvement of the stability for slower indentation rates, on the contrary the stability is slightly better for faster indentations than for slower when studying the number of required iterations.

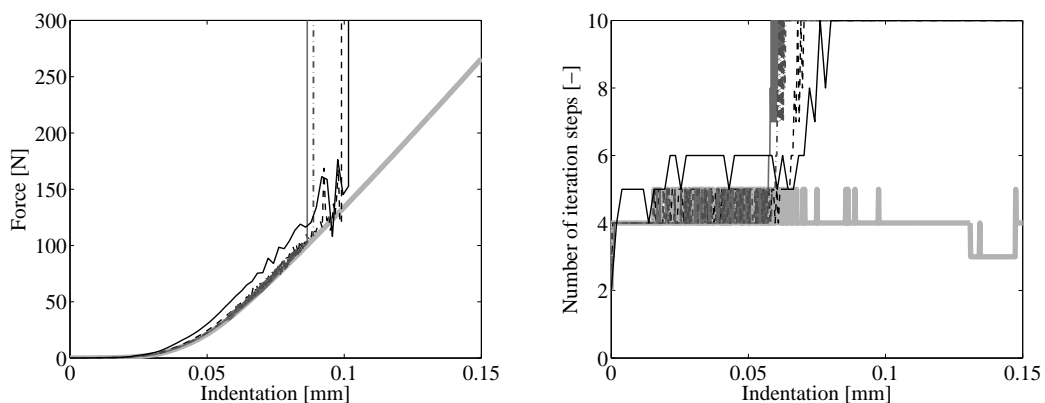


Figure 21: Contact force (left) and number of required Newton-Raphson iterations (right) as a function of indentation for dynamic conditions with different indentation rates. From slowest to fastest (markers for respective indentations in Fig. 30); solid grey (square), dash-dotted (circle), dashed (triangle) and solid black (star). quasi-static conditions (thick grey).

## 4.2 Means to increase stability

The instabilities in the dynamic calculations make it impossible to investigate the effect of approximating the system as quasi-static. Two approaches to increase stability has been investigated, increasing the time resolution of the calculations and exchanging the stiffest roughness springs for softer. By comparing quasi-static and dynamic results it can be concluded that both means proved to be efficient and giving minor effects on the results. Details about the calculations can be found in Appendix C.2.

### 4.2.1 Increase the time resolution

The large difference between the first values of the excitation point Green's function may be one of the reasons for the instability in the contact calculations. Using smaller time step gives less difference in roughness spring force for the Newton-Raphson iteration to sort out. Here is an approach tried where the sample frequency is doubled and quadrupled, corresponding to a time step of  $9.76 \cdot 10^{-6}$  and  $4.88 \cdot 10^{-6}$  seconds respectively instead of the original  $19.53 \cdot 10^{-6}$  seconds. Resampling is made with a linear interpolation between samples, Fig. 22 shows the first 25 milliseconds of the original and the new Green's functions for the excitation point and its closest neighbour(s).

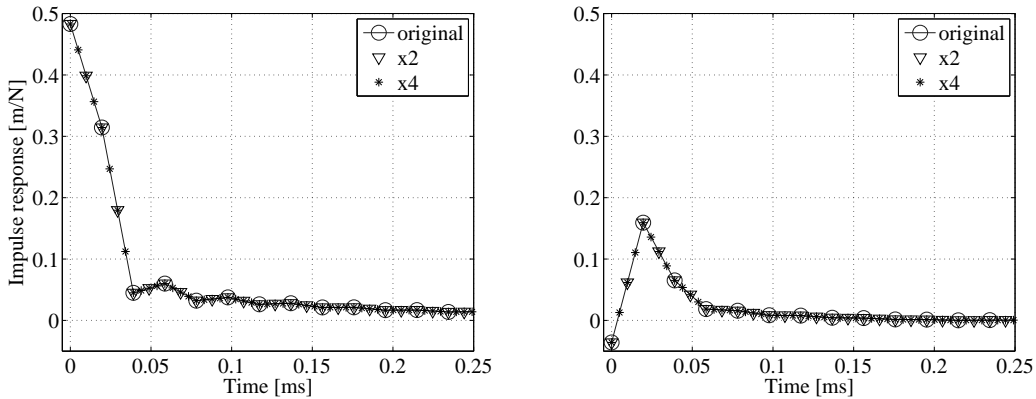


Figure 22: *Original and resampled Green's functions for the excitation point (left) and its closest neighbour(s) (right). A linear interpolation between samples is used.*

### 4.2.2 Exchange the stiffest roughness springs for softer

There is a huge spread in stiffness among the roughness springs of the road surface. As the algorithm fails when the mass-spring system is pressed down to a certain limit, corresponding to a certain compression of the roughness springs in contact, one approach to increase stability is to exchange the stiffest roughness springs for softer. The non-linearity makes it difficult to identify "the stiffest" springs, they have different stiffness in different regions of the compression. Fig. 23 shows the spring relations for the roughness springs after the exchange as black lines, the dashed lines indicates the stiffest springs that are exchanged for softer. In the figure the spring force is evaluated at a compression of  $9 \cdot 10^{-6}$  meter, the 80 springs that gives the highest spring force are replaced by the next 80. Where (compression point), what (spring force or stiffness) and how many spring relations that should be exchanged can easily be varied.

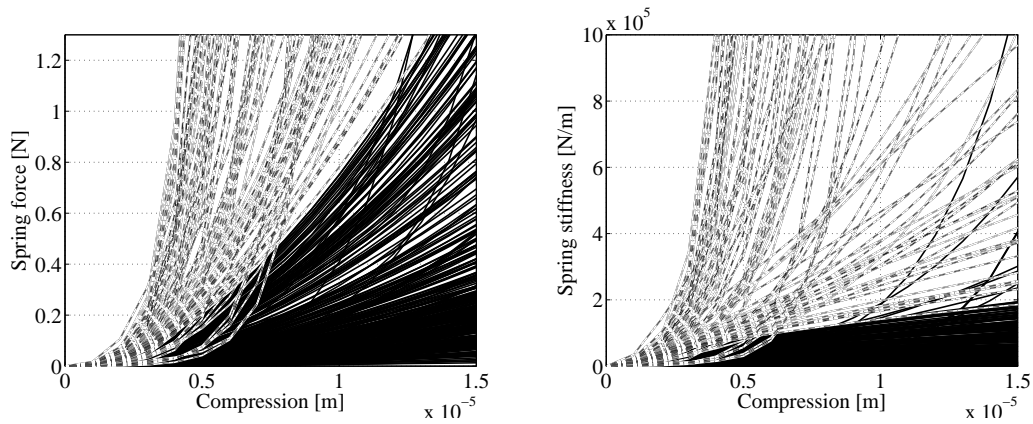


Figure 23: *Spring force and spring stiffness relations, black lines indicates the remaining relations, dashed lines indicates the stiffest springs that are exchanged for softer. The spring force is here evaluated at a compression of  $9 \cdot 10^{-6}$  meter, the 80 springs that gives the highest force are replaced by the next 80.*

#### 4.2.3 Calculation results - quasi-static conditions

The influences on the results of the means to stabilise the dynamical calculations are investigated in an quasi-static implementation, results are shown in Fig. 24-26. The deviations from the original implementation grows in general with increasing indentation but can be considered small for contact forces expected in corresponding tyre/road contact situations. The largest differences are found when exchanging the 80 stiffest springs for softer.

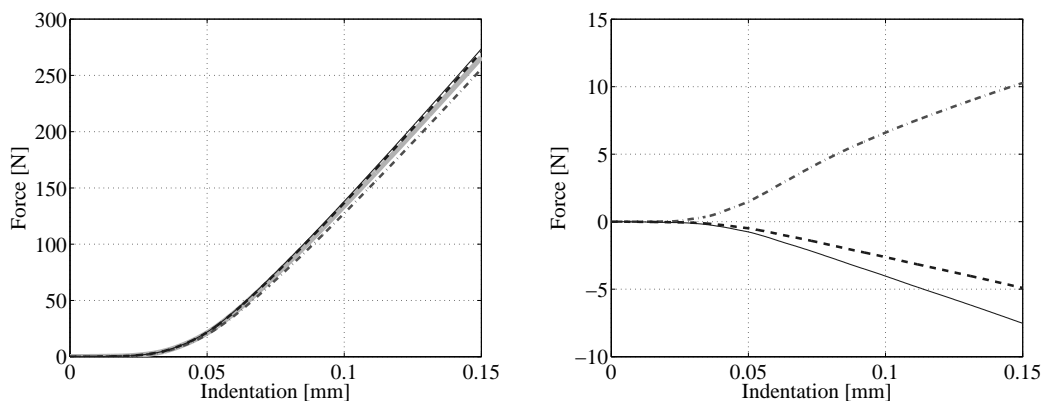


Figure 24: *quasi-static conditions: Contact force as a function of indentation (left), original implementation (thick solid grey), 2 x time resolution (dashed), 4 x time resolution (thin solid) and exchanged contact springs (dash-dotted). Difference between the original implementation and when implementing the different means (right).*

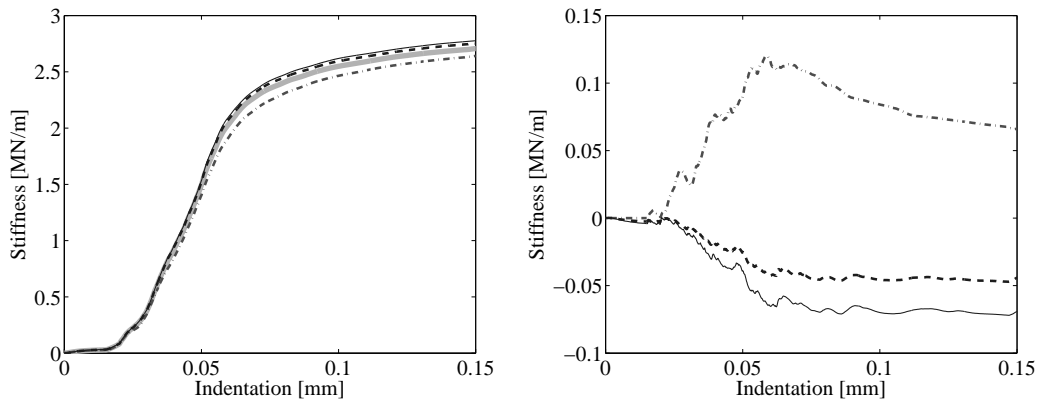


Figure 25: *quasi-static conditions: Contact stiffness as a function of indentation (left), original implementation (thick solid grey), 2 x time resolution (dashed), 4 x time resolution (thin solid) and exchanged contact springs (dash-dotted). Difference between the original implementation and when implementing the different means (right).*

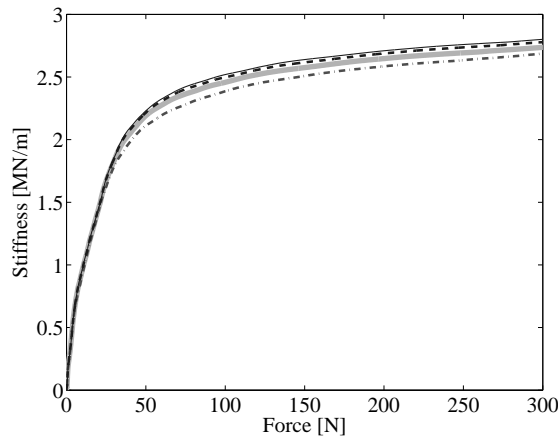


Figure 26: *quasi-static conditions: Contact stiffness as a function of contact force, original implementation (thick solid grey), 2 x time resolution (dashed), 4 x time resolution (thin solid) and exchanged contact springs (dash-dotted).*

#### 4.2.4 Calculation results - dynamic calculations

Dynamic calculation results for the original implementation and when the different means to increase stability are taken, are shown in Fig. 27-29. As the original implementation fails at an indentation of about 0.05 millimeter it is not meaningful to look at the deviations introduced by the means. Stability problems also occur when doubling the time resolution, but this happens at indentations of more than 0.12 millimeter and a contact force of 200 Newtons. Hence slightly out of range for a normal tyre/road contact situation.

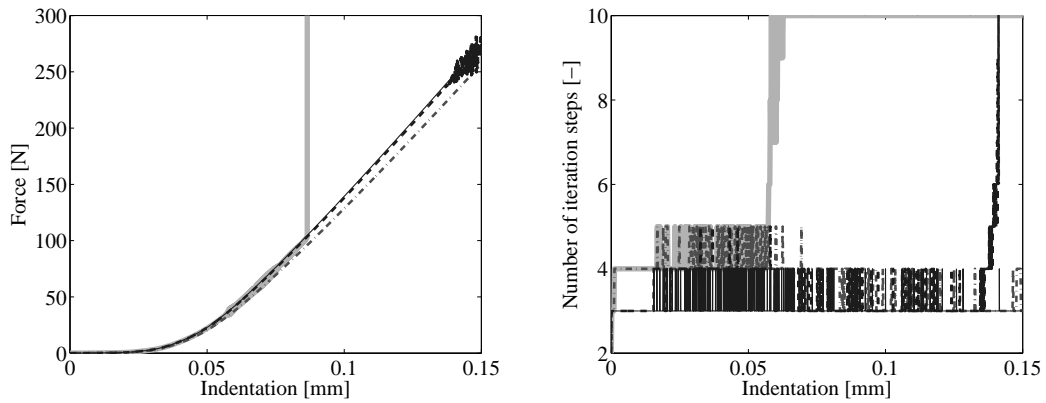


Figure 27: *Dynamic case: Contact force as a function of indentation (left), original implementation (thick solid grey), 2 x time resolution (dashed), 4 x time resolution (thin solid) and exchanged contact springs (dash-dotted). Number of required Newton-Raphson iterations as a function of indentation (right).*

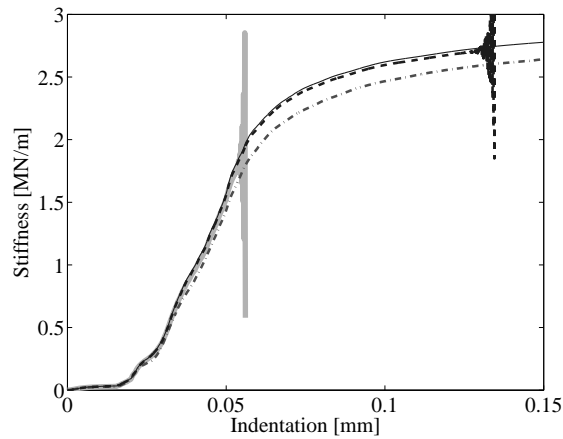


Figure 28: *Dynamic case: Contact stiffness as a function of indentation, original implementation (thick solid grey), 2 x time resolution (dashed), 4 x time resolution (thin solid) and exchanged contact springs (dash-dotted).*

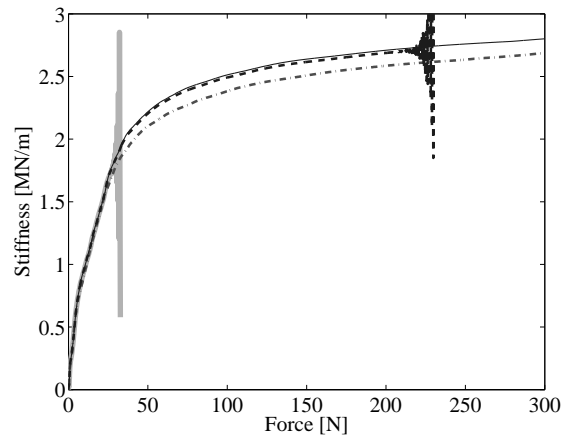


Figure 29: *Dynamic case: Contact stiffness as a function of contact force, original implementation (thick solid grey), 2 x time resolution (dashed), 4 x time resolution (thin solid) and exchanged contact springs (dash-dotted).*

### 4.3 Dynamic effects - inertia of the tread

The results of dynamic calculations will here be compared with results of the quasi-static approach. No large differences between them are found except for extreme loading rates. Two types of predetermined indentations are used, linear, which has been used so far, and quadratic, see Fig. 30. Four loading rates are used for each type. The quadratic type is tested to simulate constant acceleration;

$$x(t) = C \cdot t^2 \quad \rightarrow \quad v(t) = 2C \cdot t \quad \rightarrow \quad a(t) = 2C ,$$

where  $C$  is a constant,  $x(t)$  is displacement,  $v(t)$  speed and  $a(t)$  acceleration. If the inertia of the tread plays an important role for the macroscopic behaviour of the contact this should be most pronounced in the dynamical results with a quadratic indentation. The calculation results are very similar for the two types of indentations, possibly due to that the accelerated mass of the tread can be considered as small compared with the contact force. The resulting time record of the contact force will for both types of indentation have a non-linear initial part, after contact is established the contact force grows almost linearly with time. The time resolution is quadrupled to avoid calculation instabilities. More details about the calculations can be found in Appendix C.3.

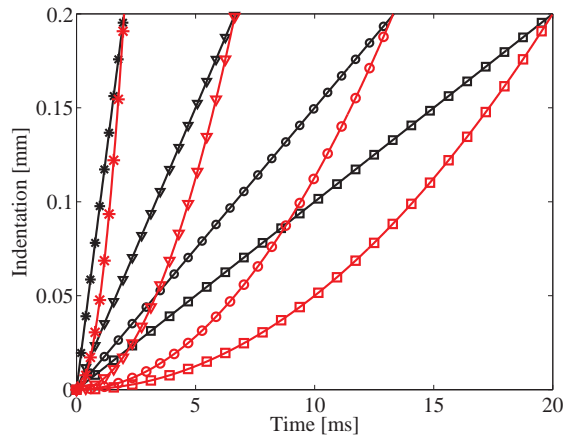


Figure 30: Two different types of predetermined indentation, linear and quadratic. Four different loading rates per type.

#### 4.3.1 Linear loading

The dynamic calculation results when using linear indentation together with the quasi-static results are shown in Fig. 31-34. The line markers connect to the predetermined indentation rates in Fig. 30, the quasi-static result is drawn with a solid grey line. The resulting loading rates are estimated from Fig. 31 by a linear fit after the the non-linear region in the beginning, they become approximately; 30, 40, 80 and 270 Newton/millisecond. It can be concluded that there are no major differences between the quasi-static and the dynamical results except for the the highest loading rate, but this has to be considered as an extreme case.

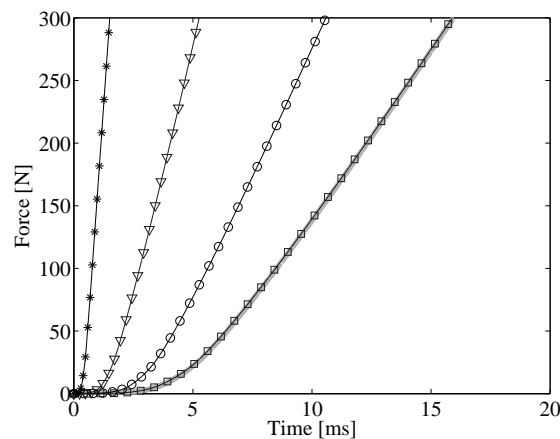


Figure 31: Contact force as a function of time (used to estimate the approximate loading rates).

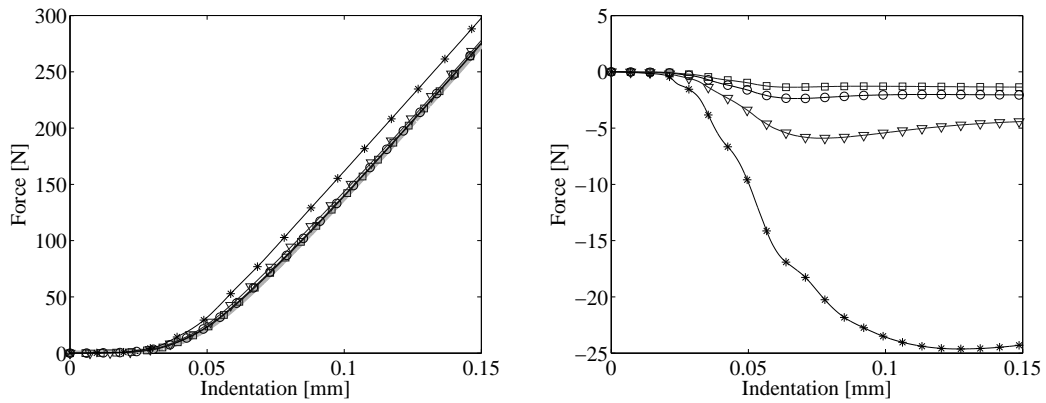


Figure 32: Contact force as a function of indentation (left), difference between quasi-static and the dynamic results (right).

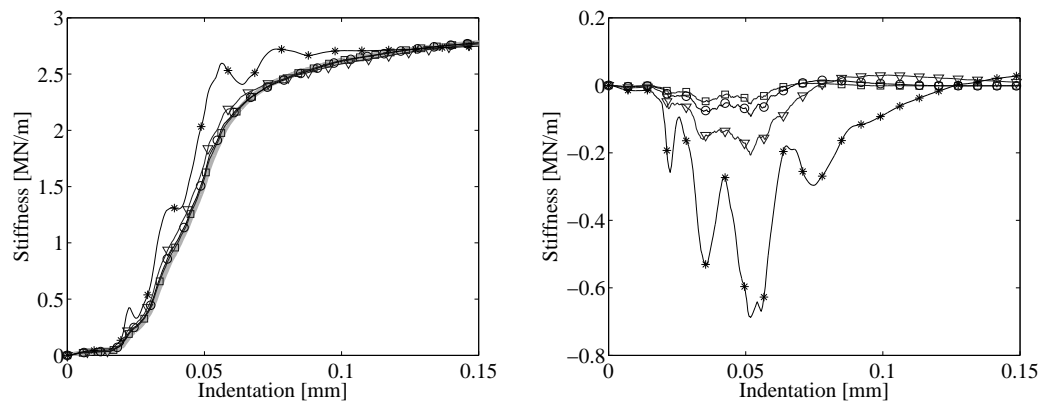


Figure 33: Contact stiffness as a function of indentation (left), difference between quasi-static and the dynamic results (right).

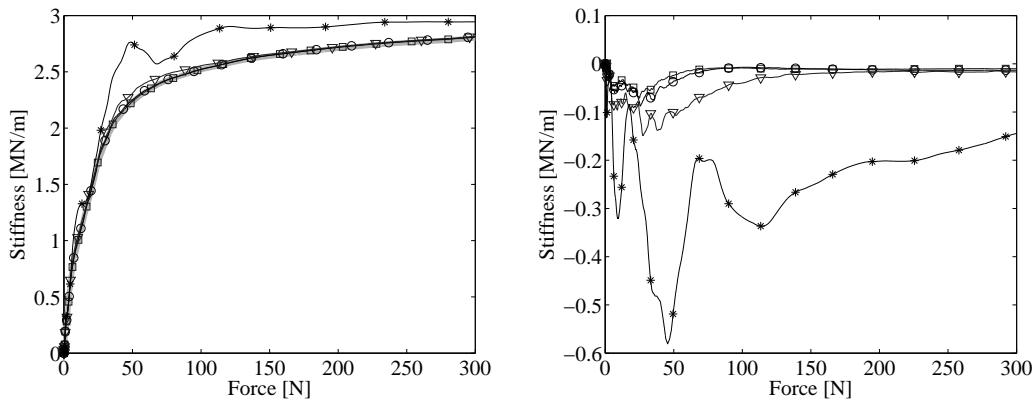


Figure 34: Contact stiffness as a function of contact force (left), difference between quasi-static and the dynamic results (right).

#### 4.3.2 Quadratic loading

Dynamic calculation results when using the quadratic type of indentation are shown in Fig. 35-38 together with the quasi-static result. The loading rates are estimated from Fig. 35 as before, they become approximately; 40, 60, 120 and 390 Newton/millisecond. It should be mentioned that it is more difficult to do a linear approximation of the curves in this case and the loading rates are hence more uncertain. As for linear indentation it can be concluded that there are no major differences between the quasi-static and the dynamical results except for the extreme loading rate.

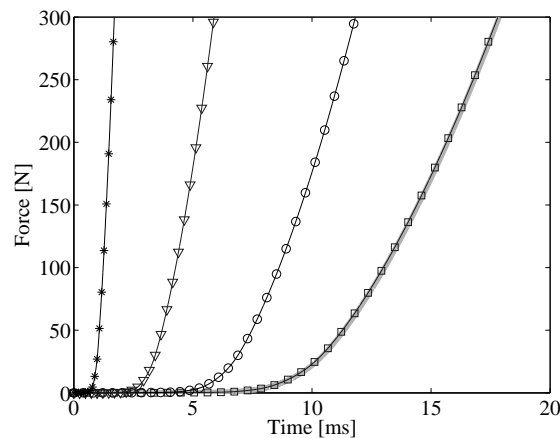


Figure 35: Contact force as a function of time (used to estimate the approximate loading rates).

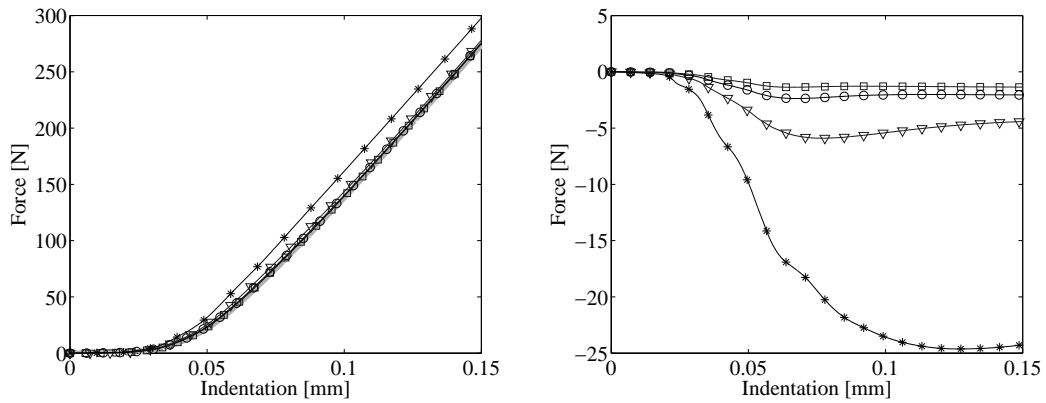


Figure 36: Contact force as a function of indentation (left), difference between quasi-static and the dynamic results (right).

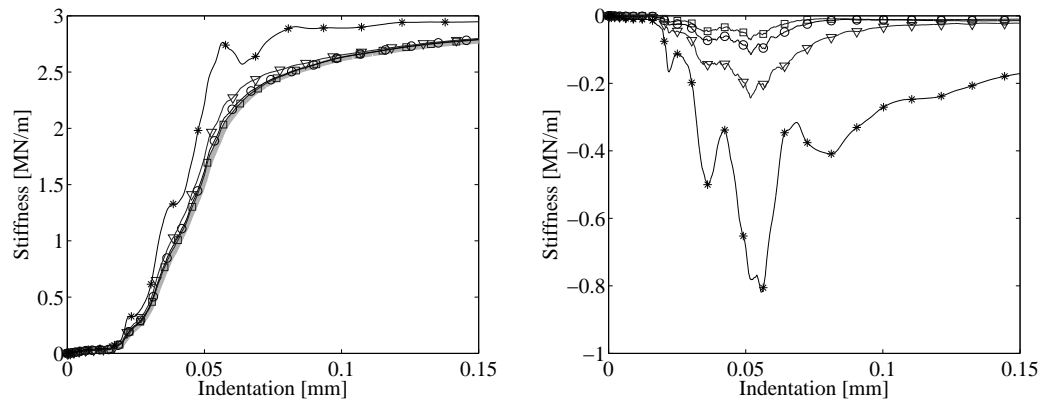


Figure 37: Contact stiffness as a function of indentation (left), difference between quasi-static and the dynamic results (right).

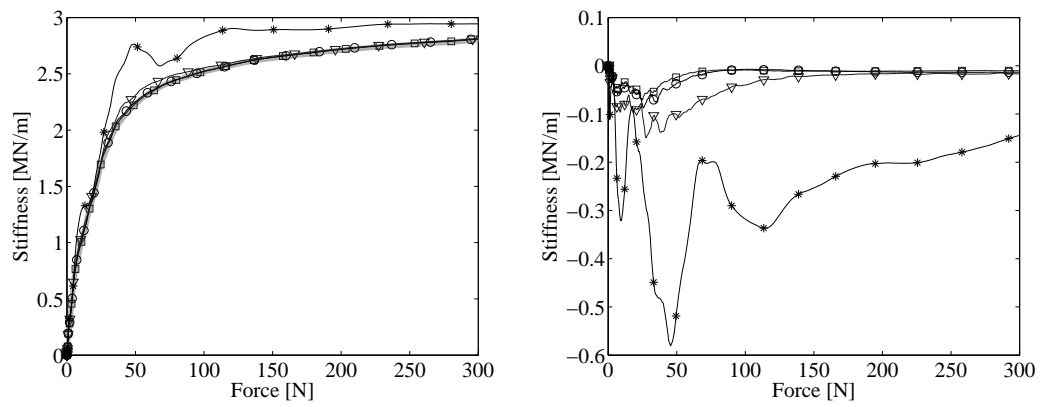


Figure 38: Contact stiffness as a function of contact force (left), difference between quasi-static and the dynamic results (right).

## 5 Introducing Adhesion

Adhesion is added to the contact model by a simple release criterion in every contact point. Comparing the results with experimental findings shows that the approach is feasible but that the model must be refined to be applicable in a tyre/road contact model and different approaches for this is briefly looked into.

### 5.1 The implementation

Adhesion is here modelled as an interfacial force acting to keep the road surface in contact with the elastic layer when the two bodies are being separated. This force has a limit, a release criterion, for which the contact break at an individual contact point and the force vanishes. The spring force-elongation and the spring stiffness-elongation relations are as first, simple approximations set as the mirror image of the original relations for compression. Fig. 39 shows the relations when the release criterion is set to 0.6 Newton which will be used as a default value in the calculations. More details about the calculations can be found in Appendix C.4.

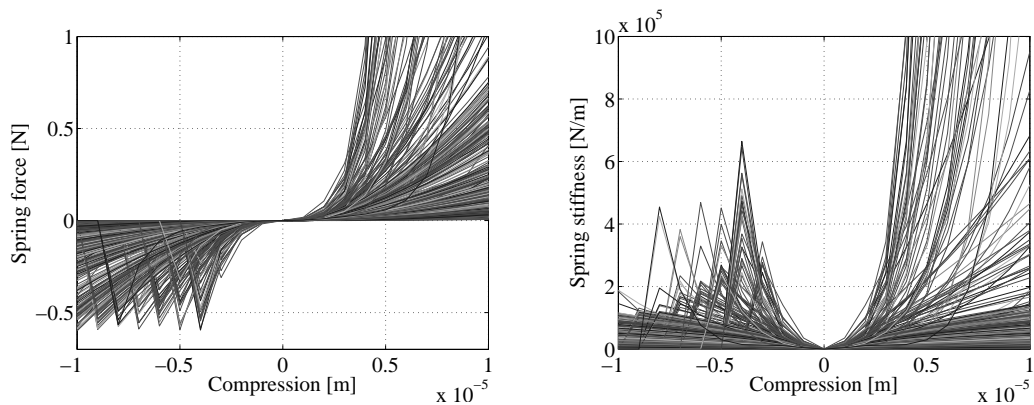


Figure 39: *Spring force (left) and stiffness (right) as a function of compression with release criterion 0.6 N.*

Even though the previous chapter showed no large deviations in the results between the quasi-static and the dynamic case, the calculations in this chapter are made for the dynamic case. To avoid the instabilities that appear in dynamical implementations of the model, the time resolution is increased by a factor 2 in the calculations.

The predetermined indentation used in the calculations involves a loading phase, a static phase and an unloading phase, an example can be seen in Fig. 40. The different phases are approximated by straight lines in the calculations. This is an unrealistic assumption for real tyre/road contact but it is here preferred because it facilitates the control of parameters like loading and unloading rate, magnitude of load and load duration.

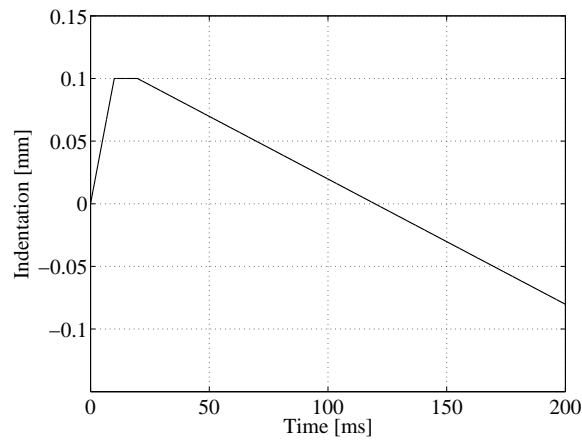


Figure 40: Example of indentation as a function of time.

## 5.2 Previous experimental results

The experimental study used for comparison in this work was conducted by Andersson and published 2009 in *Wear* [16]. In the setup, tyre tread sample blocks were loaded and rapidly unloaded from a sample of a road surface while the record of the contact force was acquired. It was concluded that the measured adherence force depends strongly on the contact geometry and area of real contact, and increases with: load, load duration and unloading rate. A contact force record from the study can be seen in Fig. 41. The figure shows the development from full loading to complete separation. The adherence force is defined as the difference between the force at time of complete separation and the minimum force. In the specific case shown in Fig. 41 a tread sample block was used with dimensions of  $30 \times 30 \times 10 \text{ mm}^3$ . The preload was 100 Newton, the load duration was 960 seconds and the unloading rate was 0.75 Newton/millisecond.

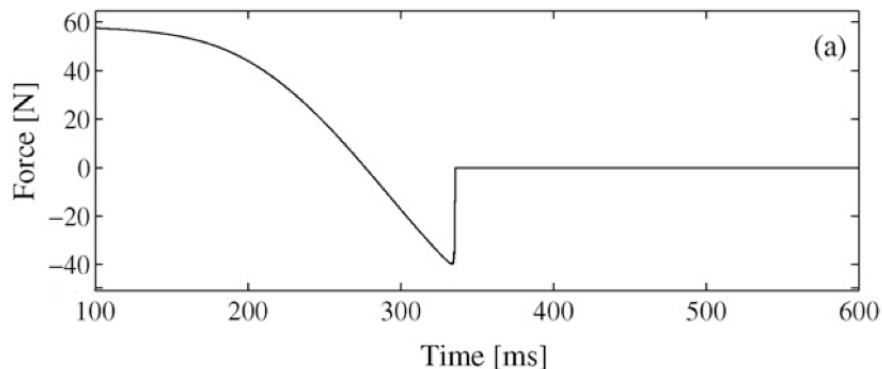


Figure 41: Total contact force as a function of time, measured force when a tread sample block is separated from a wearing coarse of a road. The original figure is taken from [16] but is here pared.

The load duration and unloading rate in the experimental case above is very long and slow when compared to a real tyre/road contact situation. When trying to model a case similar to the one in Fig. 41 with a very long load duration, problems with costly calculations start to become apparent. Fig. 42 shows the calculation result from an attempt to reconstruct a situation similar to the experimental case above. To account for the shorter load duration time, a higher load magnitude is used. The unloading rate is slightly slower in the calculated case, approximately 0.6 Newton/millisecond.

The general character of the modelled result is similar to the measured result but the abrupt release seen in Fig. 40 is missing. The release rate does not seem to increase significantly even though the force is redistributed on the remaining elements in contact when individual contacts are released, there is no big avalanche-effect.

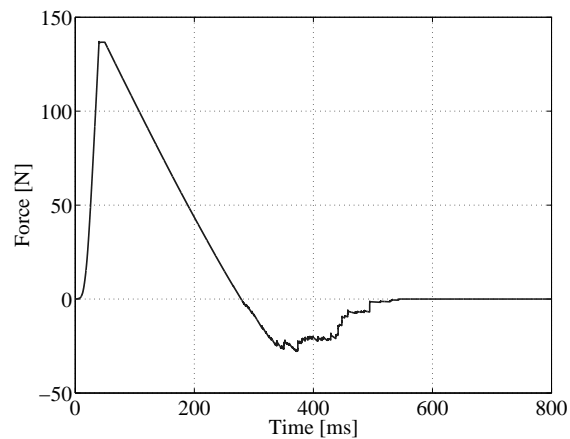


Figure 42: Contact force as a function of time, calculation with an aim of approximately reconstructing the situation from the experimental result shown in Fig. 41.

### 5.3 Brief parameter study

The present way of implementing adhesion in the contact model is here investigated by varying the parameters; release criterion, load magnitude, load duration and unloading rate. It can be expected that the first two parameters will affect the modelled adherence force, stronger bonds will give a larger adherence force and higher load will give more contact points and hence a larger adherence force.

The calculation results when varying the release criterion is shown in Fig. 43. The criteria used are 0.3, 0.6 and 0.9 Newton, the indentation as a function of time is the same in all cases. The magnitude of the adherence force is greatly affected by the release criterion but the shape of the curve is similar in all cases.

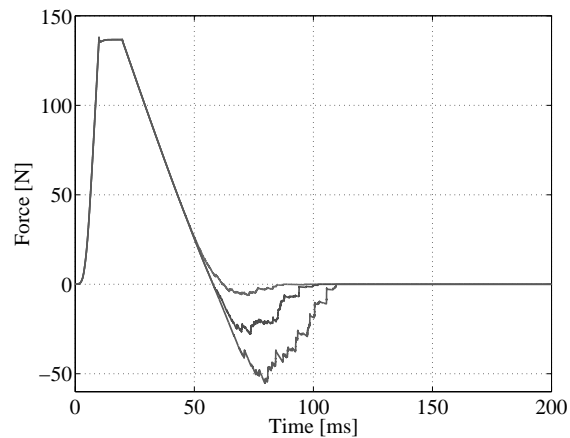


Figure 43: Calculated contact force as a function of time when using release criterion of 0.3, 0.6 and 0.9 N respectively.

Calculation results when varying the load magnitude are shown in Fig. 44 (left). This is done indirectly by varying the predetermined indentation Fig. 44 (right). The resulting maximum loads are 14, 62 and 150 Newton. The unloading rates are affected, for the three cases they become approximately 1.8, 2.4 and 3.8 Newton/millisecond respectively. The magnitude of the adherence force is affected by the load magnitude, for the three cases it is approximately 16, 23 and 28 Newtons. The appearance of the curves are very similar in all cases.

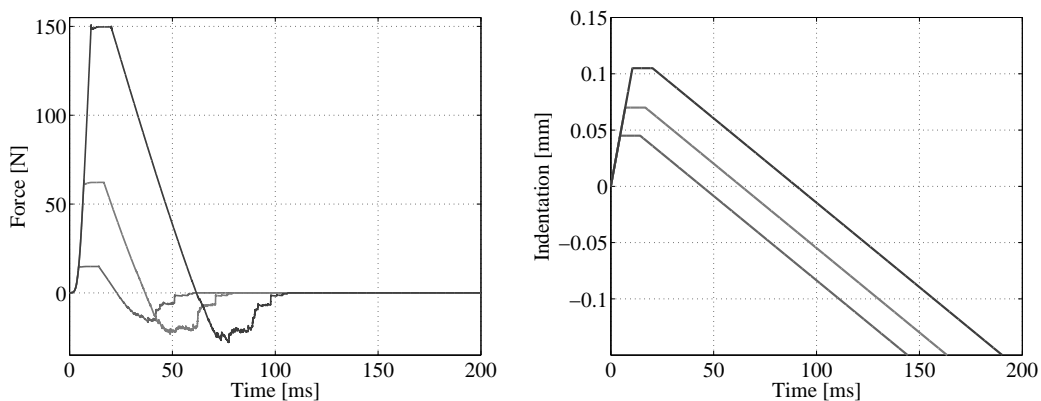


Figure 44: Left: calculated contact force as a function of time when using a load magnitude of 14, 62 and 150 N respectively. Right: the predetermined indentations as a function of time for the different cases.

Calculation results when varying the load duration are shown in Fig. 45. Load durations of approximately 1, 10 and 30 milliseconds are used, all other parameters are kept constant. The modelled adherence force is the same for the three cases. This is not surprising as there is no other time dependence in the model than the impulse response of the elastic layer.

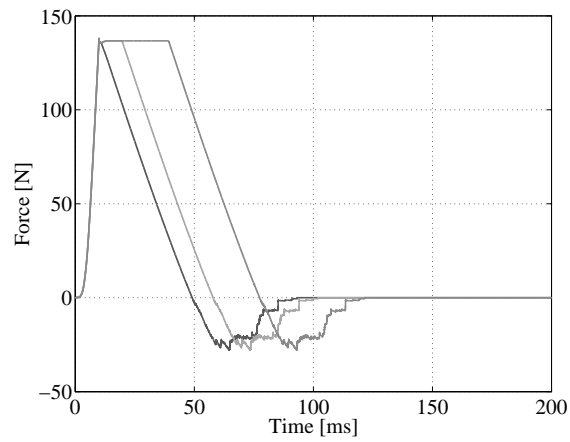


Figure 45: *Calculated contact force as a function of time when using a load duration of 1, 10 and 30 ms respectively.*

Calculation results when varying the unloading rate are shown in Fig. 46. This is done indirectly by varying the rate of the predetermined indentation in the unloading phase. Unloading rates of approximately 1.7, 2.4, 3.7, 7.2 and 24.0 Newton/millisecond are obtained, all other parameters are kept constant. The modelled adherence force is nearly the same for all cases and the present model can not capture this aspect of the experimental results of Andersson in [16].

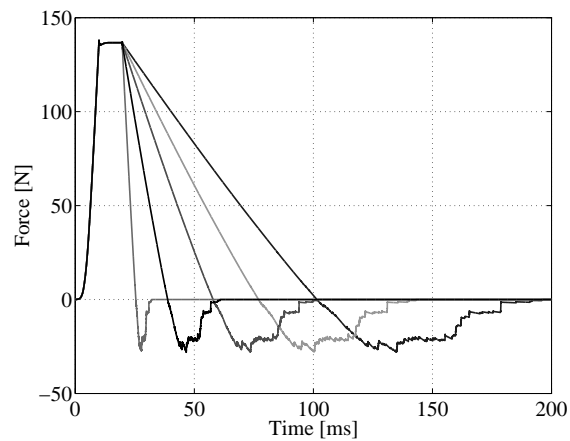


Figure 46: *Calculated contact force as a function of time for unloading rates of approximately 1.7, 2.4, 3.7, 7.2 and 24.0 N/ms.*

## 5.4 Development of the adhesion model

The adhesion model must be refined to capture the behaviour of the adherence force in the experiments of Andersson [16]. The release must be quicker, more avalanche-like in order to resemble the experimental results (Fig. 41). It is also desirable that the magnitude of the modelled adherence force will depend on load, load duration and unloading rate in the same manner as found in the experiments. The question about whether full dynamical calculations must be conducted or if it is sufficient to approximate the system as quasi-static is also briefly discussed in this chapter.

One measure to make the adhesion model more realistic is to assign different *spring force-compression* and *spring stiffness-compression* relations for the loading and the unloading phase. This can be explained with dissipation of energy, *contact hysteresis*, and the change of force equilibrium position after contact. As the indentation of one element is taken as the indentation of the outermost point within that element (see Fig. 11), the equilibrium position just when contact is established is at zero indentation. After the element has been pressed into the other body and is positioned at the zero-indentation level again, some small-scale points may still be in contact due to adhesion, Fig. 47. This will induce a total contact force on the element even though the indentation is zero. Fig. 48 shows an idea of how a spring force-compression relation for one contact spring could look like keeping in mind that this does not claim to be a valid guess. To develop a greater understanding about the roughness spring relations and how they should be implemented in a numerical contact model like the one presented in this work, both theory and experimental results should be studied and tested. Text books like Maugis [18] and Persson [19] are good starting points for this future work, more recent research can also easily be found, examples could be Buzio and Valbusa [15] and Berke [20].

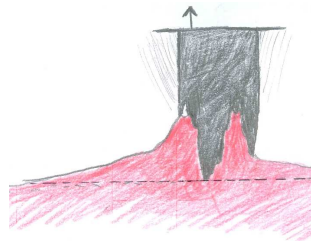


Figure 47: Schematic sketch. When adhesion forces are present, contact on small length scales may change the force equilibrium position.

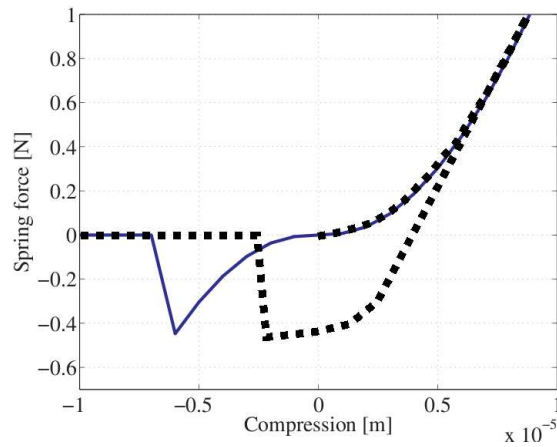


Figure 48: *Spring force-compression relations including adhesion, solid line shows the present implementation and the dotted line is an idea of how future spring relations could look like.*

The adherence force for a tread block rapidly separated from a road surface depends on parameters like load, load duration and unloading rate according to the experimental results of Andersson [16] which are supported by various adhesion contact theories (references can be found in Andersson's paper). One or several of these dependencies can relatively easily be included in the adhesion-implementation of the present contact model. A factor that grows with contact time/pressure could for example be multiplied with the release criterion for a contact point. If a point with a short contact time has a low resistance to break the connection, this could lead to a more avalanche-like rupture of the whole tread block. Improvements of the contact model, more or less, like these will be tested in a near future.

A preliminary conclusion from the previous result chapter, Ch. 4, was that the calculation result of a loading situation is very similar for a dynamic implementation and a quasi-static. At least the latter was an acceptable approximation when not working with extrem loading rates. Fig. 49 shows the result of a sinusoidal loading and unloading including an adhesive release criterion, calculated with both a dynamic and a quasi-static implementation. The character of the results are very similar, the magnitude of the adherence force is the same. Differences are mainly found in the details, when one or a group of contacts break. It seems like a quasi-static approach may be a good approximation to the dynamic process of a road surface loaded and unloaded from an elastic layer.

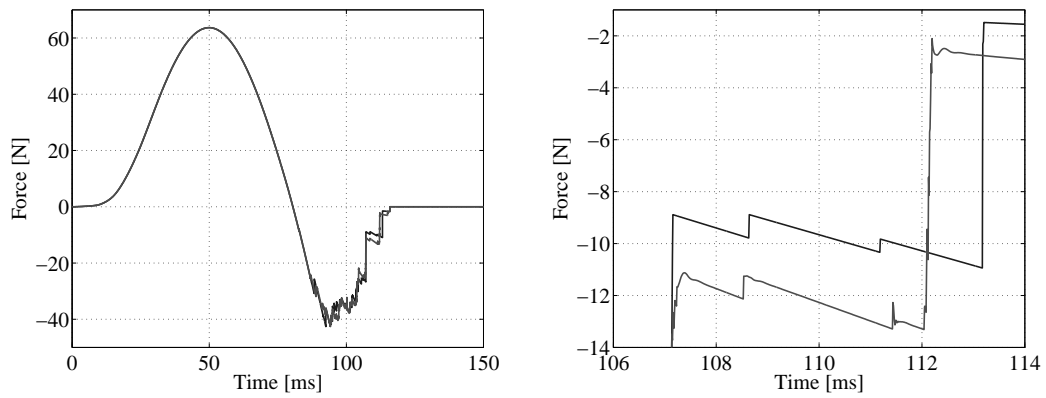


Figure 49: Calculated contact force as a function of time for a sinusoidal loading and unloading including an adhesive release criterion, quasi-static implementation (dark grey) and dynamic implementation (grey).

## 6 Discussion

The contact model presented in this study consists of a number of different parts with origins in different numerical models and calculations. The uncertainties and limitations of these parts, concerning for example material data, discretisation in time and space, different numerical implementations, are hence also present in the current model.

The numerical instability problems in the dynamic calculations are challenging, it does not help to increase number of iterations, refine the initialisation of the Newton-Raphson variable or use faster/slower indentation rates. There are though measures to increase stability where using a finer time resolution is one. This indicates that the stability problems are connected to the discretisation of the numerical model in time and space. Questions then arise weather it is feasible to calculate Green's functions for higher frequencies. In this study the time resolution of the response is increased with a linear interpolation between values, to what extent this means adding "imaginary" information can be questioned. It would be interesting to validate this resampling approach by comparing with calculations where the Green's functions of the elastic layer are actually calculated for the wanted time resolution.

Another measure to increase stability is to use softer contact springs. Even though the tests showed that exchanging the 80 stiffest springs gave the largest deviation from the original approach compared to increasing time resolution, the efficiency of this measure could probably be increased substantially. A concern about this measure is an ongoing investigation that may show that the stiffnesses of the current roughness springs are underestimated for small indentations. This implies that the stability problem will be more pronounced when using future refined versions of the contact springs. But it could also be that other zero-finding solvers would be more successful in suppressing instabilities.

Andersson found a in [16] that the adherence force depends on the unloading rate and therefor highlighted the importance of dynamic calculations: "This relation highlights the importance of including dynamic effects when describing and modelling the separation process; conclusions for quasi-static models must be handled with care". The results presented in this study implies that the need for dynamic calculations may be less than expected, at least for loading situations. Making definite conclusions at this early stage is though difficult, especially for the case of unloading as the adhesion model first must be refined. It would of course be beneficial if future investigations could show that a quasi-static approximation is sufficient for small-scale tyre/road contact modelling, as dynamical calculations turned out to be problematic with respect to numerical instabilities.

Adhesive forces are included in this study in a very brute way and comparisons with experimental results show that the approach must be refined. The planned improvements includes testing different force-compression relations for the contacts springs to see if better agreement to experiments can be obtained. A more theoretical approach to the development of the adhesion model would certainly also be of interest but not naturally more rewarding due to the complexity of the problem.

## 7 Conclusions

A numerical model describing the detailed contact between an elastic layer indented by a rough road surface has in this work been developed further (Ch. 3). In the new implementation the problem is treated dynamically and it includes non-linear contact springs and an early adhesion model. Validation of the implementation is made in Ch. 3.5 for the case of quasi-static indentation by a comparison with calculation results of Andersson [2]. The agreement is, not surprisingly, perfect as the same approach is used.

Numerical stability problems appear in the dynamic calculations when the indentation (corresponding to a certain contact force) increases above a limit (Ch. 4.1). This instability manifests itself by calculations requiring more Newton-Raphson iterations than allowed, and strange, oscillating contact behaviour. Means to increase stability of the dynamical calculations are successfully implemented in Ch. 4.2. A doubling of the time resolution would be a sufficient measure for most cases, minimising the effect on the results compared to the original implementation.

The effect of elastic layer inertia is then studied in Ch. 4.3 by different types of indentation rates, one where the indentation grows linearly and one where quadratic functions are used. The results show very similar contact behaviour for the two types. No big differences were even found between different indentation rates, except for an extreme case. It can be concluded that a quasi-static approximation is adequate for the investigated situation and spatial resolution of the contact patch.

A first step towards including adhesive forces in the contact model is made in Ch. 5 by adding a primitive contact release criterion for unloading situations. Comparisons with experimental results show that this simple approach gives a decent approximation of the adherence force but that it can not produce an avalanche-like release, and that it does not capture the dependence of load duration and unloading rate. It was concluded that the adhesion model must be further developed and suggestions were presented in Ch. 5.4.

To summarise; A contact model for tread block/road surface interaction was successfully implemented and methods to avoid instabilities in the model have been found. The model was used to show that inertia effects of the elastic layer can be considered negligible under the investigated conditions and that the tested simple release criterion simulating the effect of adhesive forces is too primitive for modelling a separation process in detail.

## 8 Future work

The instability problem in the dynamical calculations needs to be addressed further. Is it intrinsic to the discretisation of the numerical model? Could another zero-finding solver or a Newton-like method like damped Newton-Raphson be more successful? How does the instability vary with resolutions of the contact patch and other parameters? How would the instability be effected by an indentation determined by an external force acting on a mass-spring system instead of the predetermined indentation used in this work?

The results of this report implies that inertial effects of the elastic layer is of minor importance and that a quasi-static approach hence is probable to be a good approximation. But before any general conclusions can be drawn should this be investigated further. The effect of different resolutions of the contact patch should for example be studied as larger elements implies more mass and possibly more inertial effects.

It is obvious that the adhesion model must be developed further, the adhesion should depend on load and load duration and unloading rate. The present implementation could without difficulty be tested with an external force acting on a mass-spring system instead of a given indentation as this situation more resembles the situation of the experiments in [16].

An open question for future work to resolve is about the origin of the adhesion in tyre/road contact. How much can be attributed to the, yet not experimentally shown, "Atmospheric pressure effect" reported by Pinnington [11]. An experimental investigation similar to the one performed by Andersson [16] but under conditions where the air pressure could be varied would here be of great interest.

The approach with non-linear contact springs to account for the, otherwise lost, small-scale information is working well but more knowledge is needed. The output from the ongoing investigation concerning underestimation/overestimation of the stiffness when collecting all indenting asperities into one circular punch, will be valuable. Questions about possible simplifications naturally arise, can the individual springs be replaced by a set or even one mean roughness spring? Can the springs be approximated as linear?

In a longer perspective, it would be very interesting to develop the contact model presented in this report to also include tangential dynamics, then could stick-slip effects for example be tested. Connecting this small-scale contact model to the global tyre/road model is also a major future task.

## References

- [1] P.B.U. Andersson, *Modelling Interfacial Details in Tyre/Road Contact - Adhesion Forces and Non-Linear Contact Stiffness*, PhD thesis, Division of Applied Acoustics, Chalmers University of Technology, Sweden, 2005.
- [2] P.B.U. Andersson, W. Kropp, *Time domain contact model for tyre/road interaction including nonlinear contact stiffness due to small-scale roughness*, Journal of Sound and Vibration 318 (1-2) (2008) pp. 296-312.
- [3] WHO edited by B. Berglund, T. Lindvall, D.H. Schwela, *Guidelines for community noise*, World Health Organisation, Geneva, 1999.
- [4] J. Selander et al, *Long-term exposure to road traffic noise and myocardial infarction*, Epidemiology volume 20 issue 2 pp. 272-279 March 2009.
- [5] Swedish National Board of Health and Welfare, *Environmental Health Report 2009 - Extended summary*, ISBN 978-91-86301-22-4, Stockholm, April 2009.
- [6] Swedish Institute for Transport and Communications Analysis, *The development of Swedish transport through to 2020*, SIKa Report Summary 2005:6, Sweden, 2005.
- [7] Petersen M.S., Bröcker J., Enei R., Gohkale R., Granberg T., Hansen C.O., Hansen H.K., Jovanovic R., Korchenevych A., Larrea E., Leder P., Merten T., Pearman A., Rich J., Shires J., Ulied A. *Report on Scenario, Traffic Forecast and Analysis of Traffic on the TEN-T, taking into Consideration the External Dimension of the Union - Final Report*, 2009, Funded by DG TREN, Copenhagen, Denmark.
- [8] U. Sandberg, J.A. Ejsmont, *Tyre/Road Noise Reference Book*, Informex, Kista, Sweden, 1st ed., 2002.
- [9] W. Kropp, *Traffic noise and tyre modelling - progress and challenges*, Presentation at the "Queen's Anniversary Prize for Further and Higher Education", ISVR, University of Southampton, United Kingdom, 2009. Retrieved 2010-03-17 from [www.ta.chalmers.se/whatsup.php?page=semndef](http://www.ta.chalmers.se/whatsup.php?page=semndef)
- [10] SPERoN (Statistical Physical Explanation of Rolling Noise). Software developed and maintained by a consortium consisting of M+P, Müller-BBM and Division of Applied Acoustics, Chalmers University of Technology. More information is found on the webpage: [www.speron.net](http://www.speron.net)
- [11] R.J. Pinnington, *Rubber friction on rough and smooth surfaces*, Wear 267 (2009), pp. 1653-1664.
- [12] K. L. Johnson, K. Kendall, A. D. Roberts, *Surface Energy and the Contact of Elastic Solids*, Proceedings of the Royal Society of London A 324 (1971), pp. 301-313.
- [13] D.S. Grierson, E.E. Flater, R.W. Carpick, *Accounting for the JKR-DMT transition in adhesion and friction measurements with atomic force microscopy*, Journal of Adhesion Science and Technology 19 (3-5) (2005), pp. 291-311.

- 
- [14] F. Yang, *Indentation of an incompressible elastic film*, *Mechanics of Materials* 30 (1998) 275-286.
- [15] R. Buzio, U. Valbusa, *Interfacial stiffness and adhesion of randomly rough contacts probed by elastomer colloidal AFM probes*, *Journal of Physics: Condensed Matter* 20 (2008) 354014 (9pp).
- [16] P.B.U. Andersson, W. Kropp, *Rapid tyre/road separation: An experimental study of adherence forces and noise generation*, *Wear* 266 (2009) pp. 129-138.
- [17] K. Larsson, W. Kropp, *A high frequency three-dimensional tyre model based on two coupled elastic layers*, *Journal of Sound and Vibration* 253 (2002) 889-908.
- [18] D. Maugis, *Contact, Adhesion and Rupture of Elastic Solids*, ISBN 3-540-66113-1, Springer-Verlag Berlin Heidelberg, Germany, 2000.
- [19] B.N.J. Persson, *Sliding Friction - physical principles and applications*, 2nd edition, ISBN 3-540-67192-7, Springer-Verlag Berlin Heidelberg, Germany, 2000.
- [20] P.Z. Berke, *Numerical modeling of the surface and the bulk deformation in a small scale contact. Application to the nanoindentation interpretation and to the micro-manipulation.*, PhD thesis, Building, Architecture, and Town Planning (BATir) Dept., Université Libre de Bruxelles, Belgium, 2009.

## A The Newton-Raphson method

The Newton-Raphson method is one of the most common algorithms used to search the zero value of a real-valued function. Its main advantage is fast convergence if the starting point is relatively close to the searched root. Fig. 50 shows an example where we want to find the value of  $x$  that makes the function  $f$  zero, this value is denoted  $x_0$ . The procedure is straight forward: a starting point,  $x^\alpha$ , is chosen as close as possible to  $x_0$ . The derivative of the function in this point is evaluated,  $f'(x^\alpha)$  and where this straight line reaches zero is set as the next point in the iteration,  $x^{\alpha+1}$ . Then the procedure is iterated a number of times or until the error is less than a specific value. The next iteration step is given by:

$$x^{\alpha+1} = x^\alpha - \frac{f(x^\alpha)}{f'(x^\alpha)} \quad (9)$$

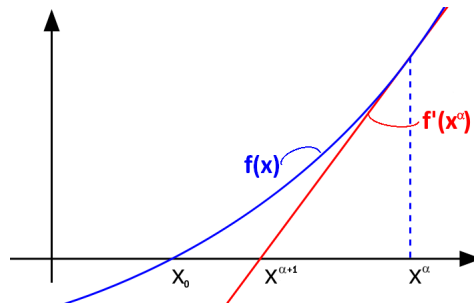


Figure 50: The root to the function  $f(x)$  can be approximated by the iterative Newton-Raphson method. A starting point is chosen and the tangent in this point is evaluated. Where the tangent intersect the  $x$ -axis is the next point in the iteration.

## **B Settings used in the calculations of the elastic layer Green's functions**

Plate dimensions: 1x1 m.

Excitation area: 2x2 cm divided into 1x1 mm parts.

In the calculations wave numbers as high as that one wavelength fits per 1x1 mm part are used.

Sample frequency: 51200

Number of samples in the Green's functions: 256

Bottom layer: aluminum material

thickness: 3 mm

density: 2700 kg/m<sup>3</sup>

Poissons ratio: 0.33

Young's modulus: constant, 72 GPa

loss factor for Young's modulus: 0.00005

Top layer: tread like material

thickness: 1 cm

density: 1300 kg/m<sup>3</sup>

Poissons ratio: 0.499

Young's modulus: frequency dependent, 25 MPa at 0 Hz. For higher frequencies the module is adapted to data from a Continental tyre. This is available up to 1 600 Hz, above this the values are slightly improvised. At high frequencies constant at 50 MPa.

loss factor for Young's modulus: frequency dependent, between 0.005 at 10 Hz to 0.55 at 50 kHz

## C Settings and .m-code used in the contact calculations

### DEFAULT VAULES:

Sampling:

sample frequency: 51200 Hz

number of time steps: 1024

Roughness springs:

scaling of the E-module:  $k\_scale = 100e5$  ;

Predetermined indentation:

Linear, from 0 to 0.2 mm in 6.7 ms, displayed in Fig. 30 with triangular markers.

Newton-Raphson iteration:

maximum number of iteration steps: 10

error limit:  $10^{-15}$ ;

initialisation: in the first NR-step set the compression of the roughness springs to their final value in the previous time step.

### C.1 Dynamic calculations with stability problems

Fig. 19: default settings

Fig. 20: Refined initialisation of the compressions of the roughness springs tested as a linear interpolation of the values in the last two time steps.

Fig. 21: Different rates of linear predetermined indentation tested, seen in Fig. 30.

### C.2 Means to increase stability

**Increase time resolution:**

sample frequency:  $2*51200$  and  $4*51200$  Hz

number of time steps:  $2*1024$  and  $4*1024$

Code used for the resampling:

```
% A function for linear interpolation/resampling of the elastic layer
% Greens functions
% 100119 created for doubling of sample rate

function [new_gf_el] = finer_dt_linear(old_gft_el, old_Nel, old_dt)

old_gf_el = old_gft_el./old_dt;
old_t_vec = (0:old_dt:(old_Nel-1)*old_dt);

new_Nel = 2*old_Nel-1;
new_gf_el = zeros(new_Nel,length(old_gf_el(1,:)));

% odd index shall be exactly as old:
new_gf_el(1:2:new_Nel,:) = old_gf_el;
```

```

% even index should be linear interpol between the old values:
new_gf_el(2:2:new_Nel-1,:) = ((old_gf_el(1:1:old_Nel-1,:) - ...
    old_gf_el(2:1:old_Nel,:))./2) + old_gf_el(2:1:old_Nel,:);

return

```

### Exchange stiff contact springs for softer:

In this report the 80 stiffest roughness springs, evaluated at a compression of  $9e-6$  m, are exchanged for the next 80 when sorting them by spring force.

Code used for the exchange:

```

%-----
%% Exchange the stiffest spring for the second stiffest:
%-----

[k_prim_Nkmax_plus9,Indx] = sort(k_primitive_contact(Nkmax+9,:),2,'descend');
from = [Indx(1:80)];
to = [Indx(81:160)];

k_function_contact(:,from) = k_function_contact(:,to);
k_primitive_contact(:,from) = k_primitive_contact(:,to);
N_klength(from) = N_klength(to);
%-----

```

## C.3 Dynamic effects - inertia of the tread

Sampling:

sample frequency:  $4 \times 51200$  Hz

number of time steps:  $4 \times 1024$

Predetermined indentation as displayed in Fig. 30.

Code used to predetermine the indentation:

```

%-----
%-----
%% Pre-determined displacement: d_ms_predet

d_ms_predet1 = zeros(size(t_vec));
d_ms_predet2 = d_ms_predet1;
d_ms_predet3 = d_ms_predet1;
d_ms_predet4 = d_ms_predet1;

%-----

%% LINEAR predet d_ms:
d_ms_predet1(2:end) = (-0.2e-3/Nit).*(1:(Nit-1));
d_ms_predet2(2:end) = (-0.3e-3/Nit).*(1:(Nit-1));
d_ms_predet3(2:end) = (-0.6e-3/Nit).*(1:(Nit-1));
d_ms_predet4(2:end) = (-2e-3/Nit).*(1:(Nit-1));

```

```

stop1 = Nit;%find(d_ms_predet1 <= -0.2e-3);
stop2 = find(d_ms_predet2 <= -0.2e-3);
stop3 = find(d_ms_predet3 <= -0.2e-3);
stop4 = find(d_ms_predet4 <= -0.2e-3);

%-----
%% OR:
%-----

%% QUADRATIC predet d_ms:
d_ms_predet1(1:end) = -0.5.*(t_vec.^2);
d_ms_predet2(1:end) = -1.13.*(t_vec.^2);
d_ms_predet3(1:end) = -4.5.*(t_vec.^2);
d_ms_predet4(1:end) = -50.0.*(t_vec.^2);

stop1 = Nit;%find(d_ms_predet1 <= -0.2e-3);
stop2 = find(d_ms_predet2 <= -0.2e-3);
stop3 = find(d_ms_predet3 <= -0.2e-3);
stop4 = find(d_ms_predet4 <= -0.2e-3);

%-----

d_ms_predet = d_ms_predet1;
stop = stop1;

```

## C.4 Introducing Adhesion

Sampling:

sample frequency: 2 x 51200 Hz

number of time steps: 10 x 2 x 1024 (but in Fig. 42 it is 40 x 2 x 1024)

Roughness springs: The original spring force and spring stiffness relations are mirrored in origo.

Predetermined indentation: Varying but always similar to the one showed in Fig. 40.

Release criterion: Default is 0.6 N but due to the discretisation of the roughness spring relations this will in practice be a value by estimate between 0.3 and 0.6 N.

Code used to set the adhesion parameters:

```

%-----
%% Adhesion, snap/on/off:
%-----
%% Non-adhesion at all:
%k_function_contact(1:Nkmax,:) = 0;
%k_primitive_contact(1:Nkmax,:) = 0;

%% Determine adhesion:
adh_indx = zeros(400,1);
for i = 1:400
    adh_indx(i) = find(k_primitive_contact((Nkmax:end),i) >= 0.6,1) -1;
    k_function_contact(1:(Nkmax-adh_indx(i)),i) = 0;
    k_primitive_contact(1:(Nkmax-adh_indx(i)),i) = 0;
end
%-----

```